Final Scientific Report

METHODS FOR DETERMINATION OF TRANSPORT COEFFICIENTS FROM HIGH POWER ARCS

Elektrophysikalisches Institut
Technische Hochschule München
Professor Heinz Maecker

Contract AF 61 (052)-649

CONTRACT
AF 61(052)-649

12. Oct. 1967

FINAL SCIENTIFIC REPORT

METHODS FOR DETERMINATION OF TRANSPORT COEFFICIENTS FROM HIGH POWER ARCS

1. Oct. 1962 - 31. Jan. 1967

PROFESSOR HEINZ MAECKER

AS PRINCIPAL INVESTIGATOR

ELEKTROPHYSIKALISCHES INSTITUT
DER TECHN. HOCHSCHULE MÜNCHEN
GERMANY

DISTRIBUTION OF THIS DOCUMENT IS UNLIMITED

THIS RESEARCH HAS BEEN SPONSORED IN PART BY THE
AEROSPACE RESEARCH LABORATORIES
THROUGH THE EUROPEAN OFFICE OF AEROSPACE RESEARCH, OAR,
UNITED STATES AIR FORCE UNDER CONTRACT AF 61(052)-649

CONTRACT
AF 61(052)-649

12. Oct. 1967

FINAL SCIENTIFIC REPORT

METHODS FOR DETERMINATION OF TRANSPORT COEFFICIENTS FROM HIGH POWER ARCS

1. Oct. 1962 - 31. Jan. 1967

PROFESSOR HEINZ MAECKER

AS PRINCIPAL INVESTIGATOR

ELEKTROPHYSIKALISCHES INSTITUT
DER TECHN. HOCHSCHULE MÜNCHEN
GERMANY

THIS RESEARCH HAS BEEN SPONSORED IN PART BY THE
AEROSPACE RESEARCH LABORATORIES
THROUGH THE EUROPEAN OFFICE OF AEROSPACE RESEARCH, OAR,
UNITED STATES AIR FORCE UNDER CONTRACT AF 61(052)-649

Abstract

An improved cylindrical cascade arc chamber is described in which any gas can be heated up to full ionisation and more. A distant pair of cascade discs may be used for measuring the voltage drop between them yielding the characteristic E(I). For the determination of the radiation loss a new fast recording thermo-couple has been developed. Methods for measuring the radial temperature distribution are dicussed and applied to several gases. In the argon arc absolute line intensities were determined spectroscopically by end-on observation. In this case the influence of the inhomogeneous layers and especially at elevated pressures the selfabsorption has to be regarded. The N_2-arc is observed side-on because of which ABEL's inversion has to be employed. For the H_2- arc a tube diameter of 2 mm was used to overcome the arc instabilities. The measurements of temperatures in this arc were carried out by means of the relative intensity method by LARENZ with a new procedure for the determination of the total line intensity. Temperatures up to 26 000 ^{o}K and degrees of ionisation of more than 100 % meaning partially double ionisation have been achieved in these arcs.

The reduction of the measured results is performed by means of a step-procedure yielding a series of transport functions, namely electrical conductivity $\sigma(T)$, heat flux potential S (T), thermal conductivity κ(T) and radiative emissivity u (T) without absorption, all as functions of temperature. At higher levels of current and temperature radiation absorption within the arc has to be taken into account which is discussed in detail. From the transport coefficients the involved cross-sections can be derived using the relevant transport equations of the kinetic gas theory which are given in a form appropriate for these purposes.

Thereby both experimental and theoretical procedures are available to determine transport coefficients of high temperature plasmas.

I. Introduction

For the determination of the transport coefficients in gases and plasmas of high temperatures and high degrees of ionisation methods are needed producing such high temperatures and providing a most simple geometry as to minimize the efforts for measurements and evaluations. Both these requirements are satisfied by an electric high power arc constricted in a cylindric chamber suffering a high wall load. For such a well defined arc in any chosen gas first of all the fieldstrength-current characteristic $E(I)$ and the radiation losses per unit arc length have to be measured. Secondly the radial temperature distributions for several currents as parameter $T(r,I)$ have to be determined by spectroscopie means. With these results and using Ohm's law the electric conductivity and its dependence on temperature $\sigma(T)$ can be evaluated. Thereafter the thermal conductivity as function of temperature $\lambda(T)$ using the energy equation can be derived provided the radiation losses can be neglected. If, however, the radiation plays an important role in the energy balance both emission and absorption have to be taken into account.
From the transport coefficients based on measurements the various cross sections involved in the gaskinetic formulas may be determined as final results of these investigations.

II. The cylindric cascade arc chamber.

The cascade arc chamber for a cylindric high power arc consists of a stack of isolated copper plates with central bores which form the discharge tube. Such an arrangement guarentees a good electric isolation in axial direction and, due to a very effective cooling, an intensive carry-off of heat in radial direction.

In the original form of the cascade chamber (1) the input power of the arc had been limited by the relatively large thickness of the plates. This is the case, because the arc current which either may pass through the plasma in the boring of the plates or through the plates themselves, thereby building a new anode- and cathode spot, chooses the way of lower voltage drop. It can be observed at high arc currents, that when very thick discs are used, a part of the current passes through the plates which thereby are damaged at the points of attachment.

Therefore it is necessary to reduce the thickness of the plates, whereby the voltage drop over one plate is decreased and the shunt over the plates is inhibited.

In the former device in each plate the coolant had been running around the shell of the central boring. At higher load the formation of vapor and the centrifugal forces had removed the water from the heated wall of the channel causing thermal isolation of the hot shell. This can be avoided by a waterduct which seen from the heat sourse is bended convexly.

The central part of a cascade disc (fig. 1) consists of a copper plate of 22 mm diam. with a central hole. From aside four slits are milled in with a circular saw-blade up to 1 mm from the central hole. So a star-like solid copper piece with four prongs remains in the center of the plate. Into this slit the two parts of a brass-plate with engraved water channels are inserted. After having put together these parts water channels are formed 4 mm wide at their ends and 1mm wide in the bended parts near the boring. By that construction the water is accelerated near the channel and pressed towards the hot wall. The cascade plate is covered by two sheets of brass which have a central boring as well as four holes of 10 mm diam. for the water supply. The whole device is silver-soldered; afterwards it is turned down to a thickness of 2 mm. The final form of the cascade plate is a square of 50 x 50 mm^2. For the assembling of the entire cascade chamber (fig. 2) flat silicon rubber rings of about 20 mm diam. and 5 mm thick are put between two neighbouring plates concentrically in order to tighten the channel to the outside space. The holes for the water supply are surrounded by pararubber rings. Distance masks made of hard paper 0,3 mm thick guarantee an equal distance between the plates in the compressed state. and inhibit the gaskets from expanding at elevated pressures. The side-on-observation can be carried out by a slit between two plates. For that purpose a radial shaft with inclined walls for a larger aperture must be milled into the discs. A specially formed gasket is used to tighten the observation window.

The entire cascade pile is terminated by two identical copper housings with a central bore of 20 mm diam. and a tube with a window for end-on-observation. The water supply is performed by four borings of 10 mm diam. parallel to the axis. Moreoverthere are four radial holes through which the isolated electrodes can be brought in. The cavities of both electrodes vessels are connected by two insulating equalization lines of large cross section in order to provide a quick compensation of possible pressure differences, and to prevent a gas flow through the arc channel.

Both equalisation tubes are furnished with a supply pipe and a very small exit hole for the gas renewal, so that only weak gas flows are possible which moreover pass outside the arc channel.

Experiments have shown that the electrodes must be brought as close as possible to the ends of the cascade tube in order to guarantee a stable arc discharge. Moreover the load limit is given by the tungsten electrodes rather than by the cascade plates. For both reasons four isolated tungsten electrodes each provided with its own ballast resistor are placed in radial direction in such a position that their fronts form a sort of continuation of the cascade tube. Each electrode consists of a tungsten rod of 4 to 10 mm diam. depending on the load and is soldered on a water cooled copper tube. Each electrode is fixed gastight and isolated inside the radial guiding hole of the electrode housing. A too intensive cooling of the electrode caused by shortening of the tungsten rod has to be avoided, because very small electrode spots are built thereby from which disturbing tungsten vapor jets might be ejected. By the very intense cooling and the reduced thickness of the plates an elevation of the power input limit is achieved. In a cascade channel with a boring of 5 mm diam. it is now possible to invest continuously a power of 18kw/cm arc length corresponding to a wall load of 12 kw/cm^2 and in a cascade of 2 mm diam. a power input of 12,5 kw/cm corresponding 20 kw/cm^2.

The cascade arc chamber can be used without any vessel for any gas and at elevated pressure (to date up to 20 atm.). Side-on as well as end-on observation is feasable. By positioning the electrode close to the cascade-ends the influence of the inhomogeneous layers can be minimized.

III E-I-Characteristic Measurements

The improved arc chamber facilitates the measurements of the E-I-characteristic considerably. Since now there is no difficulty to connect any of the plates with an electronic circuit from outside the potential drop in the arc column between any two chosen plates can easily be measured. In order to establish a good connection from the arc column to the probe plates an electron current of 150-200 mA is impressed from the arc to each of the probe plates. Exact equality of the two currents is necessary for the elimination of inaccuracies in the field strength measurements. This equality is controlled automatically by an appropriate electronic device which stabilises the absolute value of each current with a maximum deviation of less than 0,5 %. For the exclusion of errors caused by bias currents flowing through the cooling water the cascade is devided into two sections of ten plates each, both cooled by separate cooling circuits. Since each of the probe plates belongs to a different section of the cascade, the resistance between the probes is some megohms. Besides, the probe plates are arranged sufficiently far away from the end plates as to eliminate any influence of disturbances due to the electrodes.

The E-I-characteristic is recorded by an X-Y-recorder, the X-deflection being controlled by the arc current I, the Y-deflection by the field strength E. By running the current through the interval of interest characteristic measurements were performed at the 5 mm-arc in N_2 in the current range from 3 to 500 A shown in fig. 3.

Furthermore characteristics were measured in H_2 at the 5 mm-arc for currents from 10 to 25 A and at the 2 mm-arc for 15-155 A, because in the 5 mm channel the H_2-arc becomes instable for currents higher than 25 A as discussed below.

Characteristics for different values of the channel diameter can be converted into each other by means of scaling laws provided local thermal equilibrium exists and radiation losses may be neglected.

Fig. 4 shows a characteristic for H_2 which is composed of measurements at 2mm, 5mm and 20mm diameter, the latter two converted to 2mm diameter. For the regions marked by dashed lines no measurements have been carried out so far but they will be accomplished in the next future.

For the measurements in the various ranges of arc current different sets of electrodes with appropriate ballast resistors for each electrode were used as to achieve a symmetical current distribution over the electrodes. An axially mounted electrode of 5...10 mm diameter was chosen for the current range up to 10 A, for the range 10 ...100 A four thin electrodes (4...5 mm diam.) radially directed were used, whereas thick radial electrodes (10 mm diam.) have been employed for currents higher than 100 A. The thick electrodes turned out to be unsuitable for currents less than 100 A because due to the small load of each electrode the arc current was no longer distributed equally to the four electrodes.

Some difficulties which arose during the characteristic measurements could be overcome. For example, the N_2-arc showed statistically instabilities in the range from 30 to 70 A; these could be avoided by providing a thick pressure equalisation connection between the electrode housings, and by reducing the gas flow to a minimum as already mentioned before. In addition large buffer vessels were connected to both electrode housings in order to damp acustic oscillations. So a stable operation of the N_2-arc could be achieved also in the range from 30 to 70 A.

In Argon two different modes of discharge have been observed for currents less than 20 A. Only one of these yields the true characteristic of the argon arc, the other one may possibly be ascribed to a low voltage arc. Furthermore, the argon arc exhibits oscillations when operated with impressed probe currents at arc currents less than 30 A.

Another difficulty occured during the measurement on the H_2-arc. The high electric field strength belonging to low current values sometimes caused a flash-over between neighboured cascade plates. Besides, for low currents in H_2 the differential resistance has high negative values so that the total system arc-power supply began oscillating. The latter difficulty can be overcome only by providing sufficiently high ballast resistors damping out these H-F-oscillations and stabilising the total system.

In spite of all precautions trouble arises during the characteristic measurements at low currents affecting the accuracy of the measurements

which thereby is not better than 4 %. This disturbances are due to small statistical "jumps" of the field strength causing a small parallel shift of the plotted curve. Jumps of the same type occur when the voltage between two probes is recorded in dependence of probe current for constant arc current. These perturbations are possibly due to an electrode phenomenon at the probe: The impressed probe current sometimes forms a spot at the electrode and sometimes it covers all the surface of the probe, depending on arc current and probe current. At the moment a method is being developed which is hoped to suspend all these difficulties.

IV. Radiation Measurements

For the measurement of the power radiated from cylindrical arcs, a new radiation thermo-couple had to be developed since the commercial devices turned out to be too slow for continuous recording the radiated power in dependence of arc current. Moreover, the sensitivity of all commercial devices is too small and not constant over an area sufficiently large for mapping the arc cross-section.

The setup of the thermo-couple is as follows: A 1...2 μ thick Al_2O_3-foil suspended in an aluminum frame bears thin layers of the thermo-metals Bi and Sb deposited on the foil by vacuum evaporation. The sheets have a shape like fingers at a hand interfering with each other. This is achieved by appropriate masks in the vapour beam. A sufficiently large area of constant sensitivity was achieved by choosing the length and the width of the fingers properly. In order to blacken the surface of the couple a further Sb-layer is evaporated but at a pressure of 0,5 mm Hg thus producing a nearly 100 % absorbing cover. Moreover, the receiving surface is placed in the center of a concave mirror reflecting the scattered radiation back to the receiving surface. The light to be measured enters the device by a central slit in the mirror. The electrical connections to the element are made from contacting silver. The new thermo-couple is free of the disadvantages mentioned above. The rise-time is about 40...80 milliseconds, the sensitivity is 0,2 volts/watt, and is constant over an area of 2 x 0,7 mm^2 whereas the arc is represented on an area of 1,6 x 0,1 mm^2 only.

The measurement of the radiation is carried out side-on through a slot as small as 0,3 x 5 mm^2, so that no disturbance of the arc can occur. The arc cross section is focussed in a reduced measure on the thermo-couple by a quartz achromate. This arrangement yields a good total sensitivity; but it is applicable only, if an area of constant sensitivity on the thermo-couple exists. Examples of radiation measurements are shown in fig. 6.

V. The radial temperature distribution in argon arcs.

The temperature measurements in an argon arc have been carried out with a cascade chamber of 5 mm diam. Some precautions were met for applications at elevated pressures up to 25 atm. The end-on temperature measurements are performed with a Zeiss-Jena grating spectrograph (dispersion ≈ 7 A/mm). A 1:1 image of the arc is formed on the entrance slit of the spectrograph. In the focal plane of the imaging lens, a diaphragm with a hole diameter of 1mm limits the aperture of the light beam to 1:70 (telecentric system). This set-up provides a correlation between each point of a spectral line with one certain radius of the arc channel. A series of different exposures (making use of a rotating sector) is taken of the argon arc, then the cascade arc is replaced by a standard carbon arc, so that calibrated intensity marks are formed on the same photoplate using the same optical system. The analysis of the line and continuum intensities is performed with a microdensitometer.

In a transparent plasma, temperatures may be determined by measuring the absolute intensity I_L of a line. The relation between I_L and the temperature T is given by

$$I_L = \frac{1}{4\pi} A_n^m n \frac{g_m}{Z} e^{-E_m/KT} h\nu l$$

where

A_n^m = transition probability
n = number density of the emitting particles
g_m = statistical weight of the upper level
Z = partition function of the emitting particle
l = length of the emitting layer

Below the normal temperature T_n (for argon: $T_{n,\,atom} \approx 15,000\ ^oK$, $T_{n,\,first\ ion} \approx 21,000\ ^oK$), I_L is a sensitive function of T which makes this intensity to a suitable thermometer for the temperature range of the investigated arc. The radial temperature distribution has been determined using the lines:

A I 4300 A with $A_n^m = 3.1 \times 10^5 \text{ sec}^{-1}$

A II 4637 A with $A_n^m = 64 \times 10^5 \text{ sec}^{-1}$

In addition to these line measurements, the temperature was also derived from the continuum intensity I_K:

SCHLÜTER gives the following expression for I_K:

$$I_K = 1.65 \times 10^{-28} \frac{n_e n_i}{\lambda^2 T_e} \left\{ \frac{6 \xi}{Z_1} (1 - e^{h\nu/kT}) + e^{-h\nu/kT} \right\} l$$

where

Z_1 = partition function of the ion

T_e = electron temperature

$\xi(\nu)$ = correction factor

The continuum intensity is less sensitive to the temperature than the line intensity.

Corresponding to the function $\xi(\nu)$ determined by SCHLÜTER, the value $\xi = 2$ has been used for the calculation of I_K at 4300 Å.

One difficulty with end-on observation of the cascade arc is that the length l of the emitting column is composed of the sum of the useful cascade length plus the (unknown) disturbance length of the inhomogeneous electrode regions.

High pressure arc spectroscopy also raises the question of self-absorption in the plasma. Before the equations above can be applied to a temperature measurement, it has to be proven that the optical depth $\chi_\nu l$ of the plasma is small compared to unity. This can be tested by applying a method which has been used in a slightly different way by JÜRGENS.

The frequency-dependent intensity over the range of one spectral line may be written:

$$I_\nu = B_\nu (1 - e^{-\chi_\nu l})$$

where

B_ν = Kirchhoff - Planck-function

χ_ν = absorption coefficient

If this equation is applied to arcs with two different lengths l_1 and l_2 ($l_2 > l_1$), χ_ν can be eliminated:

$$I_{\nu 2} = B_\nu \left[1 - \left(1 - \frac{I_{\nu 1}}{B_\nu}\right)^{l_2/l_1} \right]$$

Assuming at first the optical depth $\chi_\nu \, l_1 \ll 1$ and therefore $I_{\nu 1} \ll B_\nu$, the series expansion may be cut off to yield

$$I_{\nu 2} = \frac{l_2}{l_1} I_{\nu 1}$$

In a logarithmic plot, the fuction $I_{\nu 2}$ ($I_{\nu 1}$), with the assumptions made above, is a 45° straight line which intersects the ordinate at the point $\ln l_2/l_1$.

If the optical depth is $\chi_\nu \, l_1 \gg 1$, both intensities $I_{\nu 1}$ and $I_{\nu 2}$ are equal the Kirchhoff-Planck function B_ν. In the logarithmic representation $I_{\nu 2}$ ($I_{\nu 1}$) this fact signifies that the function ends on that 45° straight line which runs through the origin.

In plotting the measured frequency-dependent line intensities, it has been proven by this method that the atmospheric pressure argon plasma is optically thin for the considered lines. In the case of the 5 atm plasma (fig. 7), the line center showed a slight absorption which could be corrected.

On the other hand, this method allows the determination of the point $\ln l_2/l_1$ on the ordinate. The difference $l_2 - l_1$ is known from the experiment (number of cascadeplates); therefore l_2 and l_1, the effective arc lengths, can be determined.

These measurements have been performed with 12 and 22 cascade plates, the corresponding difference $l_2 - l_1$ is equal to 23 mm. At 500 A arc current, the ratio of the lengths has been determined to be $l_1/l_2 = 1.55$ resulting in an effective length of 7 mm for each of the inhomogeneous layers at the cascade ends.

A method for the determination of the required atomic constants for temperature measurements has been discribed by RICHTER; this method also helps to prove the existence of an optically thin plasma.

The procedure consists of a logarithmic plot of the calculated total intensities of two spectral lines (one of them may be replaced by the continuum intensity anywhere) against each other. The result is a function in which the temperature T is parameter. When the measured values are then inserted in this diagram, and if they fit the theoretical curve, the accuracy of the required constants and the transparent emission is proved and the same time, the temperature can be determined.

In figs. 8 and 9 line and continuum intensities of an atmospheric pressure arc and of a 5 atm arc have been plotted and show good agreement between measured values and theoretical predictions. For the ion line A II 4348 Å a transition probability of $A_n^m = 11,5.\ 10^7\ sec^{-1}$ has been used, corresponding to the value given by OLSEN.

Figs. 10 and 11 show the measured radial temperature distribution across the argon arc at two different pressures (1 atm and 5 atm) for various arc currents. From fig. 11 it can be seen, that the high pressure arc has a flatter temperature profile than the atmospheric pressure arc.

VI. Temperature Measurements in the N_2-Arc.

For the investigations on the N_2-arc a cascade of 5 mm diam. has been used. The maximum arc current can be raised up to 550 A. It is limited by the melting of the anode tungsten rods (12mm diam.) rather than by the thermal loading capability of the plates. The arc is observed side-on through the 0.3 mm slit between two neighbouring cascade plates. For this purpose an observation port with an aperture of approximately 1 : 10 and a closing window is installed. To gurantee a black background a second observation port is provided opposite to the first one with a window inclined in such a way that the reflected image of the arc does not arrive at the path of observation. For measuring the radial temperature distribution at various currents the intensities of proper lines were registered by means of a plane grating spectrograph (PGS 2, Jenaoptik). Above 20.000 ^{o}K the nitrogen spectrum fig. 12 contains besides a few N I lines mainly N II lines and the spectral distribution changes only slightly for higher temperatures. Above 450 A single N III lines are observed too. Due to this order of line type appearence the cross-section of the arc in end-on observation shows up a blue colour at low currents from the molecular radiation; at currents above 20 A the well known white core appears emitted from the atoms and electrons. At currents higher than 300 A a new violet core arises within the first one originating from the ions.

For the determination of the radial temperature distributions the absolute intensities of the N I line 4935 Å and the N II lines 3995 Å, 4488 Å, 5045 Å have been measured calibrated by means of the standard arc with data according to H. MAGDEBURG and U. SCHLEY. The corresponding transition probabilities were taken from the book by H. R. GRIEM. The resulting radial temperature distributions for arc currents varied in steps of 50 A are shown in fig. 13. In fig. 14 the axial temperatures are plotted versus the arc current. Additional values taken from measurements by H. MAECKER are inserted too. The highest temperature achieved in N_2 is 26 000^{o}K corresponding to degree of ionisation of 125 %. These radial temperature distributions are used together with the E-I-characteristic to evaluate the electrical conductivity $\sigma(T)$. As a first result the $\sigma(T)$ curve is shown in fig. 15 together with a theoretical curve according to YOS.

VII. Radial temperature distributions in the H_2-arc.

The H_2-arc in a cascade chamber of 5 mm diam. shows up great instabilities both inside the channel and in the electrode regions at currents above 25 A.

In order to overcome these instabilities it was to clarify whether they arise from perturbations in the electrode regions or whether they are a feature of the arc column itself. Therefore the H_2-arc was run in a cascade chamber consisting of one channel with 2 mm diam. at each end near the electrodes and with a tube of 5 mm diam. in the middle of the cascade (fig. 16). Each cross-section of these three parts were focussed on a drum camera. Such exposures (fig. 17) show clearly the column in the 5 mm diam. part to be unstable at currents above 25 A although the column in the 2 mm diam. parts of the cascade are entirely stable up to highest arc currents employed. It is abvious that under these circumstances perturbations in the electrode regions can not affect the arc column. Therefore it has to be concluded that the instabilities of the H_2-arc column are a phenomenon of the column itself.

The onset of the instabilities occurs at currents depending on the cascade bore as it is shown in the following table.

10 mm diam. arc	instabilities above	10.5 A
5 mm diam. arc	instabilities above	25 A
3 mm diam. arc	instabilities above	70 A
2 mm diam. arc	instabilities above	150 A

With a cascade bore of 2 mm diam. it is possible to operate a steady H_2-arc up to high powers. Therefore the measurements of the radial temperature distribution were performed with a 2 mm cascade.

The used cascade arc chamber is assembled by 24 plates 2 mm thick. Radial temperature distributions are measured spectroscopically at arc currents up to 150 A. The input power of 11.7 kw/cm corresponds to a wall load of 18.6 kw/cm^2. In the 2 mm diam. tube the axis temperatures at currents above 60 A exceed 16 000°K. The intensity of the lines and of the continuum in the hydrogen spectrum have a maximum at a temperature of 16 000°K and decrease again with higher temperatures

(fig. 18). Therefore the intensity in an arc has a maximum at a certain radius which moves outwards with increasing currents while a growing depression in the axis of the arc occurs (fig. 19 and 20). Measuring an intensity distribution like this from side-on is not reasonable, because the errors of the resulting axial intensities are too large due to the necessary ABEL's inversion. Therefore the observation end-on has been preferred. In this case the two following requirements have to be satisfied. On the one hand the observation beam has to be kept precisely parallel to the axis of the arc and on the other hand the whole length of the column has to be mapped exactly on the slit of the spectrograph. This is realized in a good approximation by a telecentric lay-out with an aperture as small as 1 : 330 . Furthermore it is important to ascertain that the inhomogenous layers in the electrode regions do not contribute essentially to the measured intensity. Indeed this influence can be neglected up to about 100 A. Above this current the inhomogeneous layers contribute a notable amount to the intensity especially in the axis of the arc, because above 16000°K the specific intensity of the column becomes smaller than that of the inhomogeneous layers. To eliminate this error difference measurements have been carried out using a short arc cascade consisting of 8 plates besides the long arc cascade formed by 24 plates. Subtracting both the intensities from each other the contribution of the inhomogeneous layers is cancelled as long as the inhomogeneous layers are not altered by the change of the cascade length.

Due to the occurence of this maximum at 16000°K it is possible according to LARENZ to determine the distribution of the absolute temperature from relative intensity measurements. If the measured relative intensity of H_β as function of the radius is related to the maximum intensity, the absolute temperature as function of the radius can be deduced from that ratio in connection with the dependence of related intensity on temperature (fig. 18). The advantage of relative measurements compared with absolute ones is that no errors caused by standard light sources and reduction filters or by other absorption losses affect the evaluation of the temperature.

Instead of determining the line intensity of H_β for a certain radius by integration along the wavelength, a procedure is applied which excludes uncertainties due to the strong line broadening in connection with the error

in the determination of the background level. The evaluation relies on the fact that the normalized line profile remains virtually unchanged for the range of temperature and electron density under consideration as theory and experiment confirm. The total intensity results from the theoretical line profile the area of which being equal to unity by a uniform extension of the abscissa and by another one of the ordinate until congruence with the measured profile is achieved. Practically this is performed by shifting the theoretical curve in a double logarithmic plot until it matches the measured profile. The total intensity is given by the product of the shifting factors in both of the coordinate directions.

The radial temperature distribution obtained in this way for arc currents of 20 to 150 A are shown in fig. 21. The highest value of temperature is 26000 ^{o}K corresponding to virtually full ionization. For comparison to our results a temperature profile measured by MOTSCHMANN in a 5 mm diam. cascade at 20 A and reduced to a cascade of 2 mm diam. by means of the scaling law is added.

VIII. Determination of material functions from characteristic measurements.

The behaviour of a cylindrical arc discharge is governed by ELENBAAS-HELLER's differential equation, which describes the balance between the energy produced within a volume element by OHM's heating and the energy lost by heat conduction and radiation:

$$\sigma E^2 - u + \frac{1}{r}\frac{d}{dr}\left(r \cdot \varkappa \frac{dT}{dr}\right) = 0 \qquad (1)$$

The term u is the emission of energy per unit volume and time, which is an unique function of temperature.

If the material functions $\sigma(T)$, $\varkappa(T)$ are known, this equation can be used, to compute the integral characteristics of an arc discharge $E(I)$ and $U(I)$, i.e. the electrical field strength and the total radiation (dependent) on arc current, as well as the radial temperature distributions $T(r, I)$. While it is interesting to compare the results of such computations with experimental values, it is more important, to use the measured $E(I)$-, $U(I)$- and $T(r, I)$-curves to determine the material functions of the arc gas with help of ELENBAAS-HELLER's energy equation. Several approximative methods have been described to compute $\sigma(T)$ and the heat flux potential $S(T) = \int_0^T \varkappa \, dT$ from the integral characteristics and the temperature distributions using a special functional dependence of on S. In this chapter a way is described by which $\sigma(S)$, $u(S)$ and $S(r, I)$ can be directely determined from the integral characteristic using the integrated energy balance equation. The following is only a brief review of the method and its results for nitrogen and argon, as it is already published in detail (A. Monterde-Garcia: Z. Physik, 181, 317 (1964)).

After introduction of the heat flux potential S and the relative radius $\varrho = r/R$ the energy equation reads:

$$\frac{R^2}{4}\left(\sigma E^2 - u\right) = -\frac{d}{d\varrho^2}\left(\varrho^2 \frac{dS}{d\varrho^2}\right). \qquad (1a)$$

There are two more equations, connecting the integral values U and I with the gas properties:

$$U = \pi R^2 \int_0^1 u \, d\varrho^2, \qquad (2)$$

$$I = \pi R^2 \int_0^1 j \, d\varrho^2 = \pi R^2 E \int_0^1 \sigma \, d\varrho^2 \qquad (3)$$

Division through E yields the conductance per length of arc, G:

$$G = \pi R^2 \int_0^1 \sigma \, d\varrho^2 \qquad (3a)$$

In a I - ϱ^2 - diagram iso-S-curves can be drawn (fig. 22). Since S, σ and u are unique functions of temperature, the iso-T, σ and u-curves coincide with the iso-S-curves.

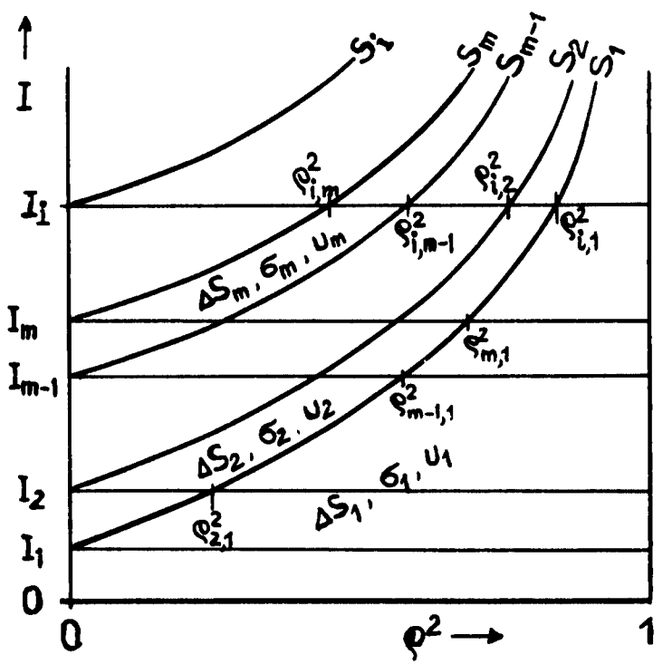

Fig. 22: Iso-curves in the I- ϱ^2-diagram.

The I- ϱ^2- plane extends from $\varrho^2 = 0$ to $\varrho^2 = 1$, and from I = 0 up to unlimited I-values. It is assumed that S equals zero at the tube wall, i. e. for $\varrho^2 = 1$, and for zero current: $S_{J=0} \neq 0$; $S_{\varrho^2=1} = 0$.

The whole plane is devided into small regions by horizontal straight lines I_i = const. and by several S_k = const. -lines, which originate in the

axis ($\varrho^2 = 0$) at the current $I = I_k$. The points of intersection between these both families have the radii $\varrho^2_{i,k}$.
Going along a straight line I_i = const. from $\varrho^2 = 1$ to $\varrho^2 = 0$ the index k in $\varrho^2_{i,k}$ is running from k = 0 at the wall to k = i in the axis.
In the stripe between two consecutive S_k-curves, S_k and S_{k-1}, particularly at the current I_i between $\varrho^2_{i,k}$ and $\varrho^2_{i,k-1}$ σ and u are postulated to be constant and are marked by the index k, i.e. σ_k, u_k.
Under this condition formula (2) and (3a) can be transformed:

$$U_i = \pi R^2 \left\{ u_i \varrho^2_{i,i-1} + \sum_{j=1}^{j=i-1} u_j \left(\varrho^2_{i,j-1} - \varrho^2_{i,j} \right) \right\}, \qquad (2a)$$

$$G_i = \pi R^2 \left\{ \sigma_i \varrho^2_{i,i-1} + \sum_{j=1}^{j=i-1} \sigma_j \left(\varrho^2_{i,j-1} - \varrho^2_{i,j} \right) \right\}. \qquad (3c)$$

For the inmost ϱ^2-interval, i.e. between $\varrho^2_{ii}(=0)$ and $\varrho^2_{i,i-1}$ the energy balance equation reads:

$$\pi R^2 \left(\sigma_i E^2 - u_i \right) \varrho^2_{i,i-1} = 4\pi \left(S_i - S_{i-1} \right). \qquad (1b)$$

For all other intervals the energy balance equation can be transformed into

$$A x + B \left(1 - e^{-x} - x \right) = C, \qquad (1c)$$

where

$$A = I_i E - U_i - \pi R^2 \sum_{j=1}^{j=k-1} \left(\sigma_j E^2 - u_j \right) \left(\varrho^2_{i,j-1} - \varrho^2_{i,j} \right),$$

$$B = \pi R^2 \left(\sigma_k E^2 - u_k \right) \varrho^2_{i,k-1},$$

$$x = \ln \left(\varrho^2_{i,k-1} / \varrho^2_{i,k} \right),$$

$$C = 4\pi \left(S_k - S_{k-1} \right).$$

The evaluation is started at the lowest I-value, I_1, for which σ and u are assumed constant over the whole radius. There u_1, σ_1 as well as $S_1 = S(I_1, \varrho^2 = 0)$ can be computed according to (2a), (3c) and (1b).

Progressing step by step to higher current values, at I_m all S-values except that in the axis, i.e. S_m, and the σ- and u-values for all intervals $\varrho^2_{m,k} - \varrho^2_{m,k-1}$ except the one bordering on the axis are known from the step I_{m-1}. Therefore at this current I_m all intersection points $\varrho^2_{i,k}$ can be computed with the help of (1c) going step by step from the outmost intervall to the axis. The still unknown quantities u_m and σ_m in the inmost interval can than be computed using (2a) and (3c) and with these values the increase in S, i.e. $S_m - S_{m-1}$ and thereby S_m from (1b). Now everything is known at the cross section $I = I_m$ = const. and the evaluation at the following current- step can be started.

In this way u(S) and σ(S) result as staircase functions, which can be smoothed out properly. At the same time S(r) is determined for every current value.

If one or more radial temperature distributions T(I, r) are measured on an arc discharge, the functional dependence S(T) can be determined comparing T (r) and S(r). This can be used to derive the temperature dependence of σ(T), as well as the thermal conductivity $\varkappa$(T) according to

$$\varkappa(T) = \frac{dS}{dT}.$$

So a procedure for evaluating transport coefficients from characteristic and temperature measurements exists, however, without considering absorption of radiation within the gas.

IX. Energy transfer by radiation.

When evaluating in the described way a strong deviation of the experimental results from the theoretical curves above a certain temperature in the case of nitrogen and argon results. It can be shown that this is mostly due to neglecting the absorption of radiative energy within the arc gas. Therefore this chapter deals with the energy transport by radiation generally and in the special case of cylindrical symmetry as given in the arc casca e.

The basic equation of an arc column is the energy balance equation:

$$\sigma E^2 - \operatorname{div} \underline{q}_S - \operatorname{div} \underline{q}_T = 0.$$

or written for cylindric symmetry:

$$\sigma E^2 - u + \frac{1}{r} \frac{d}{dr} \left(r \varkappa \frac{dT}{dr} \right) = 0.$$

σE^2 gives the gain of energy per unit volume by OHM's heating. $\underline{q}_T = -\varkappa \nabla T$ is the heat flux vector. $\underline{q}_S$ is the radiation flow vector, so that $\operatorname{div} q_S = u = e - a$ is the difference between the energy e, emitted from the unit volume, and a, the energy absorbed within it.

In former evaluations only the term e in u had been considered, i.e. the absorption of energy within the arc column had been neglected, so that $u = e(T) = u(T)$ could be taken as a unique function of temperature. In more accurate computations the term a, which is no longer a unique function of temperature, must be taken into account too.

The optical behaviour of a gas is described by the coefficients of emission and absorption:

ε_ν = coefficient of emission per unit volume, time and frequency
α_ν = coefficient of absorption of radiative energy per unit length.

Both coefficients depend very strongly on frequency. Therefore, when determining $a = \int_0^\infty \alpha_\nu \, d\nu$, the absorption per unit volume and time, first one has to compute a_ν, the absorption per unit volume, time and frequency range at a certain frequency:

$$a_\nu = \alpha_\nu(r=0) \cdot \iiint \varepsilon_\nu(r) \cdot \exp\left(- \int_0^r \alpha_\nu \, d\varrho \right) \cdot \frac{1}{r^2} \cdot dV .$$

Here r is the distance of an emitting element from the point r = 0, where the absorption a_ν is to determine.

Similar formulas for $\underline{q}_{\nu S}$ and $\underline{q}_S$ can be derived. Since the exponential in the fromula for a_ν decreases very rapidly with increasing r the main contribution to the absorption at the point r = 0 comes from emitting elements the distance of which from r = 0 is not larger than a certain length of order of magnitude $1/\alpha_\nu$. As long as α_ν and ε_ν do not change very much within this region, it is useful to represent both α_ν and ε_ν by a Taylor's series around r = 0. Inserting these into the formulas for a_ν or $q_{\nu S}$ the integration can be carried out. If the constant term in the series for α_ν and the constant and linear term in the series for ε_ν are sufficient, to describe the α_ν-curve and ε_ν-curve within the interesting region, which is the case for very strong absorption, there results a linear dependence of $\underline{q}_{\nu S}$ on ∇T, when KIRCHHOFF's law is used (representation of heat flux by a diffusion equation).

$$\underline{q}_{\nu S} = - \varkappa_{\nu S} \nabla T ; \qquad \varkappa_{\nu S} = \frac{8\pi}{3} \cdot \frac{h^2 \nu^4}{c^2 kT^2} \cdot \frac{1}{\alpha_\nu} \exp(-h\nu/kT) .$$

If higher terms in the two series have to be considered, i.e. when α_ν is smaller, direct integration for a given $\alpha_\nu(r, \vartheta, \varphi)$ dependence is more advantageous as regions with very different temperatures contribute to the absorption at a certain point.

For a very small coefficient α_ν the absorption per unit volume can be negligible small compared with the emission per unit volume in same regions of a gas, so that only the emissive term e(T) has to be considered in the energy balance equation.

In many problems direct integration of the formulas for a_ν or $\underline{q}_{\nu S}$ is necessary for a given α_ν- and ε_ν-curve, which is a very timeconsuming task. In special symmetries the formulas can be simplified. For cylindrical symmetry, as given in the cylindrical arc column, there results for a_ν :

$$\alpha_\nu(r) = - \frac{8h\nu^3}{c^2} \alpha_\nu(r) \int_0^R d\varrho \exp\left(-\frac{h\nu}{kT}\right) \alpha_\nu(\varrho) \cdot \varrho \cdot \int_0^\pi d\varphi \frac{B(d)}{\sqrt{r^2 + \varrho^2 - 2r\varrho\cos\varphi}} ,$$

where

r = distance of the absorbing element from the axis

ϱ = distance of the emitting element from the axis

R = radius of the arc tube

The integration over z could already be performed beforehand yielding the function B(d), which means a projection of the entire radiative problem into the plane z = 0.

$$B(d) = \int_1^\infty dv \frac{\exp(-vd)}{v\sqrt{v^2-1}} \; ;$$

$$B(0) = \frac{\pi}{2}$$

$$\frac{dB}{dd} = -K_0(d)$$ = modified BESSEL's function of the second typ.

d = projection of the optical length between emitting and absorbing element on the plane z = o.

$$d = \int_{Q'(\varrho,\varphi,0)}^{A(r,0,0)} \alpha_\nu \, ds$$

where ds is a line element of the connection between emitting and absorbing element, projected into the plane z = o.

As α_ν is a function of radius only it is advantageous to transfer the line element ds properly into a line element in radial direction db.

For a given distribution of T(r) and α_ν(r) one can compute a_ν(r) and e_ν(r) using these formulas.

To get a general view of the effect of absorption, sometimes it is sufficient to compute approximately a_ν (r) at some points of the arc column. For this purpose the formula for a_ν can be further simplified:

a) In the arc axis the formula for a has a special simple form:

$$a_\nu(r=0) = \alpha_\nu(r=0) \int_0^R e_\nu(\varrho) \, B(d) \, d\varrho \; ; \qquad d = \int_0^\varrho \alpha_\nu(b) \, db \, .$$

b) If the emitting region is confined to a small channel around the axis, the absorption per unit volume outside the emitting zone is given approximately by:

$$a_\nu(r) = 8\alpha_\nu(r)\cdot B(g_0)\frac{1}{r+\varrho_{max}}\cdot F\left(\frac{\pi}{2}, \frac{2\sqrt{r\varrho_{max}}}{r+\varrho_{max}}\right)\cdot\int_0^{R_S}\varepsilon_\nu(\varrho)\,\varrho\,d\varrho,$$

where $F(\chi, k)$ = LEGENDRE's normal integral of the first kind.

$$g_0 = \int_0^r \alpha_\nu(b)\,db$$

ϱ_{max} = radius, at which $\varepsilon_\nu\varrho$ has it's maximum.

c) In the case that in most parts of the column strong radiation is emitted, an aproximative formula for a_ν results, if computing the projection of the optical length, d, for a fixed r and ϱ a mean value for α_ν independent on φ, namely $\alpha_{\nu M}$, is chosen. Then a_ν can be written as:

$$a_\nu = 4\alpha_\nu\int_0^R d\varrho\;\varepsilon_\nu\,G\left(\frac{\varrho}{r}, \varrho\alpha_{\nu M}\right),$$

where $G(\varrho/r, \varrho\alpha_{\nu M})$ only depends on the two functions ϱ/r and $\varrho\alpha_{\nu M}$. For special r-, ϱ- and $\alpha_{\nu M}$-values the function $G(\varrho/r, \varrho\alpha_{\nu M})$ can be read from a diagram representing G over ϱ/r with $\varrho\alpha_{\nu M}$ as parameter.

X. Determination of average collision cross sections.

If the temperature dependence of the electrical and thermal conductivity $\sigma(T)$ and $\varkappa(T)$ are given, the average collision cross sections and their temperature dependence can be evaluated with the help of the kinetic theory of gases. For this purpose in this chapter formulas are derived for the material functions $\sigma(T)$ and $\varkappa(T)$, which thanks to special simplifications are sufficiently clear in their dependence on the different cross sections, and which yet do not deviate too strongly from the exact solutions. These formulas can be used to determine the average collision cross sections for collisions between the various particles in the gas .

Deriving formulas for the electrical conductivity σ and the thermal conductivity $\varkappa$ deviation from MAXWELL-equilibrium must be assumed for electrons as well as for heavy particles. Computing the heat conductivity of electrons $\varkappa_e$ three terms in the series of orthogonal functions describing the velocity dependence of the electron distribution function have been taken into account. In all other cases only two terms in the series of orthogonal functions are sufficient for the velocity distribution functions.

Using the Coulomb-model for collisionsbetween charged particles and the model of rigid spheres for all other collisions the different average cross sections for the collision between two types of particles s and t have been reduced to one average cross section Z_{st}. The connection with the CHAPMAN and COWLING -Ω- integral is given by:

$$Z_{st} = 8\sqrt{\frac{m_s m_t}{2kT(m_s+m_t)}}\cdot\Omega^{(1)}_{st}(1) .$$

The resulting formulas for the material functions are compiled in the following sections:

a) Electrical conductivity:

$$\sigma = \frac{3}{2}\cdot\frac{n_e e^2}{\sqrt{2kTm_e}}\cdot\frac{1}{Z_{ae}n_a + Z_{ie}n_e + Z_{em}n_m}\cdot\varrho_\sigma ,$$

where

$$\varrho_\sigma = \frac{A^2 + 1.697A + 0.697}{0.517A^2 + 2.019A + 0.644} , \qquad A = \frac{Z_{ie}n_e}{Z_{ae}n_a} .$$

b) Heat conductivity in the dissociation region

$$\varkappa = \varkappa_a + \varkappa_m + \varkappa_D ;$$

$$\varkappa_a = \frac{75}{16} k \sqrt{\frac{kT}{m_a}} \cdot \frac{9\sqrt{6}\, Z_{mm} + 41\, Z_{am}\cdot (n_a/m_m) + \frac{27}{2} Z_{am}}{9\sqrt{6}\, Z_{mm} Z_{aa} + 41 \frac{n_a}{n_m} Z_{am} Z_{aa} + \frac{113\sqrt{2}}{4} \frac{n_m}{n_a} Z_{am} Z_{aa} + \frac{976\sqrt{3}}{27} Z_{am}^2} ;$$

$$\varkappa_m = \frac{75}{16} k \sqrt{\frac{kT}{m_a}} \cdot \frac{9\sqrt{6}\, Z_{aa} + \left(\frac{113}{4} \cdot \frac{n_m}{n_a} + \frac{27}{2}\right) Z_{am}}{9\sqrt{6}\, Z_{mm} Z_{aa} + 41 \frac{n_a}{n_m} Z_{am} Z_{aa} + \frac{113\sqrt{2}}{4} \frac{n_m}{n_a} Z_{am} Z_{aa} + \frac{976\sqrt{3}}{27} Z_{am}^2} ;$$

$$\varkappa_D = \frac{3}{4} \sqrt{\frac{3k}{m_a T}} \cdot D(T) \cdot \frac{n_a}{n_a + 2n_m} \cdot \frac{1}{Z_{am}} \cdot \left(1 + \frac{T}{n_a} \frac{dn_a}{dT}\right),$$

where $D(T) = \frac{5}{2} kT + U_D + 2u_a - u_m$.

$\varkappa_a$ and $\varkappa_m$ are the common contact heat conductivities due to atoms and molecules, $\varkappa_D$ is the heat conductivity caused by diffusion flows. D(T) represents the energy necessary for one dissociation process.

c) Heat conductivity in the ionisation region

$$\varkappa = \varkappa_a + \varkappa_i + \varkappa_e + \varkappa_I$$

$$\varkappa_a = \frac{75}{16} k \sqrt{\frac{kT}{m_a}} \cdot n_a \frac{32\, Z_{ii}\, n_e + (59 n_a + 27 n_e) Z_{ia}}{32 Z_{ii} Z_{aa} n_a n_e + 59 Z_{ai} (Z_{ii} n_e^2 + Z_{aa} n_a^2) + 86 Z_{ai}^2 n_a n_e} ;$$

$$\varkappa_e = \frac{75}{16} k \sqrt{\frac{kT}{2m_e}} \cdot n_e \cdot \frac{1}{8\sqrt{2}\, n_e Z_{ee} + 26 (n_e Z_{ei} + n_a Z_{ea})} \cdot \varphi_\varkappa ,$$

$$\varphi_\varkappa = \frac{A^2 + 1.28\, A + 0.405}{0{,}432\, A^2 + 1{,}43\, A + 0{,}365} ;$$

$$\varkappa_I = 3 \sqrt{\frac{k}{m_a T}} \cdot I(T) \cdot \frac{n_e}{n_e + n_a} \cdot \frac{1}{Z_{ai}} \left(1 + \frac{T}{n_e} \frac{dn_e}{dT}\right),$$

$$I(T) = \frac{5}{2} kT + U_I + u_i - u_a .$$

In the ionisation region the heat conductivity consists of the contact heat conductivities by atoms, ions and electrons $\varkappa_a$, $\varkappa_i$ and $\varkappa_e$ and $\varkappa_I$, the heat conductivity due to energy transport by ambipolar diffusion processes. Generally $\varkappa_i$ can be neglected in comparison with $\varkappa_e$. I(T) represents the energy needed for one total ionisation process.

As in regions of different degree of ionisation different collision processes play an important role, and as the temperature dependence of the material functions is much more influenced by the ratios of the particle densities than by the cross sections, one can evaluate the unknown functions Z_{st}(T) from σ(T) and $\varkappa$(T). From σ(T) the Coulomb cross sections $Z_{ei} = Z_{ii} = Z_{ee}$ and also Z_{ea} can be determined. Interpreting the heat conductivity $\varkappa$ one notices, that in the reaction regions the cross sections for the collision between the reacting particles play the dominating role, i. e. Z_{ai} in the ionisation peak and Z_{am} in the dissociation peak. In the intermediate region Z_{aa} can be determined with the help of extrapolation and iteration.

XI. Concluding remarks.

With the new cascade arc chamber a useful tool is created for heating a gas up to full ionisation and even more in a simple geometry i. e. in cylindrical symmetry with inhomogeneous ends as small as possible. A method for measuring the E(I)-characteristic has been developed displaying a good reproducibility of both the arc itself and the measuring device. For the radiation measurements a new type of a fast thermocouple with high sensitivity was constructed. Procedures of precise temperature measurements were tried out and applied to arcs in various gases. Also the theory for evaluating transport coefficients from the results of measurements has been improved particularly by taking the absorption of radiation within the arc into consideration. Finally the gaskinetic formulas for the transport coefficients were revised to give the best approximation for arc conditions. So all suppositions for carrying out the required measurements and for evaluating these results to obtain the transport coefficients and the various cross-sections involved are established.

The papers related to this research work (but by parts supported by other institutions) which are published already in scientific journals, are listed below:

H. MAECKER. S. STEINBERGER und M. URBAN:

Eine Kaskadenbogenkammer für sehr hohe Leistungen.
Z. f. angew. Phys. 15, 440 (1963)

A. MONTERDE-GARCIA:

Materialfunktionen von Bogenplasmen aus Charakteristikenmessungen.
Z. Physik 181, 317 (1964)

U. BAUDER:

Temperaturmessungen am Argon-Hochleistungsbogen.
Z. Physik 205, 303 (1967)

W. HERMANN und A. MONTERDE-GARCIA:

Bestimmung von Wirkungsquerschnitten aus Messungen an zylindrischen Kaskadenbögen.
Z. Physik 205, 313(1967)

H. MAECKER und S. STEINBERGER:

Weiterentwicklung der Kaskadenbogenkammer für hohe Leistungen.
Z. angew. Phys. 23, (1967)

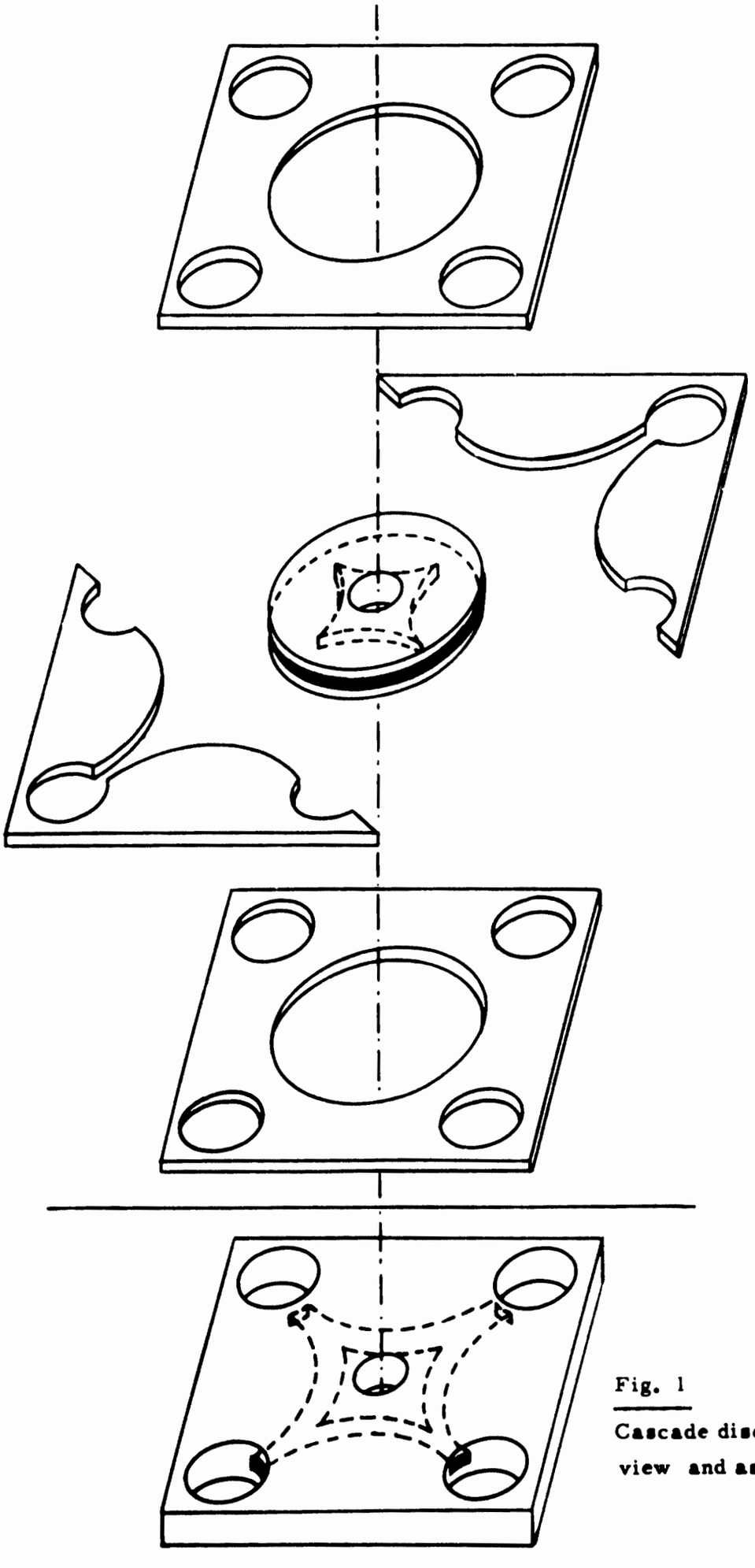

Fig. 1

Cascade disc, exploded view and assembled

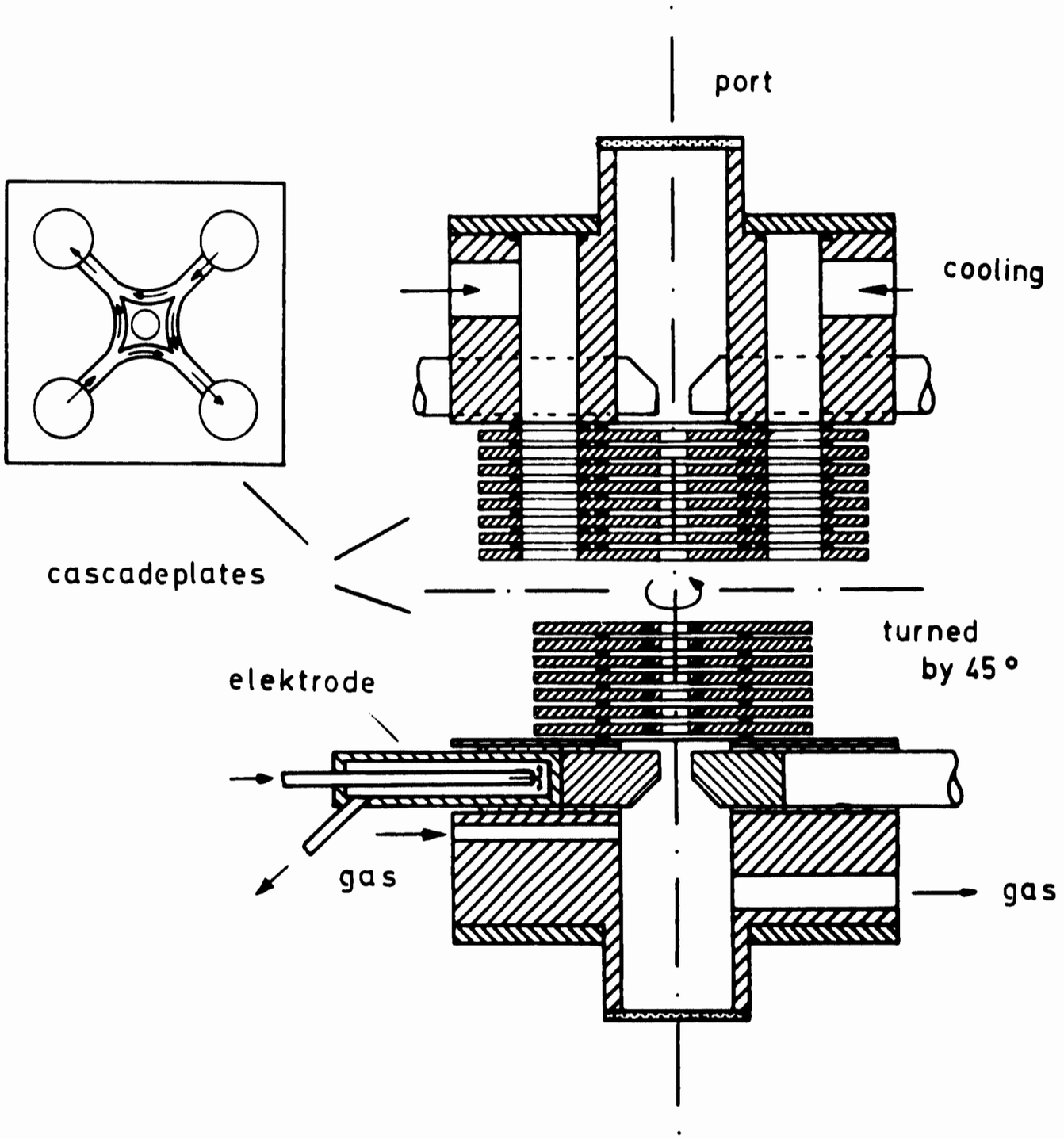

Fig. 2 Cascade arc chamber in two parts turned against each other by 45 °

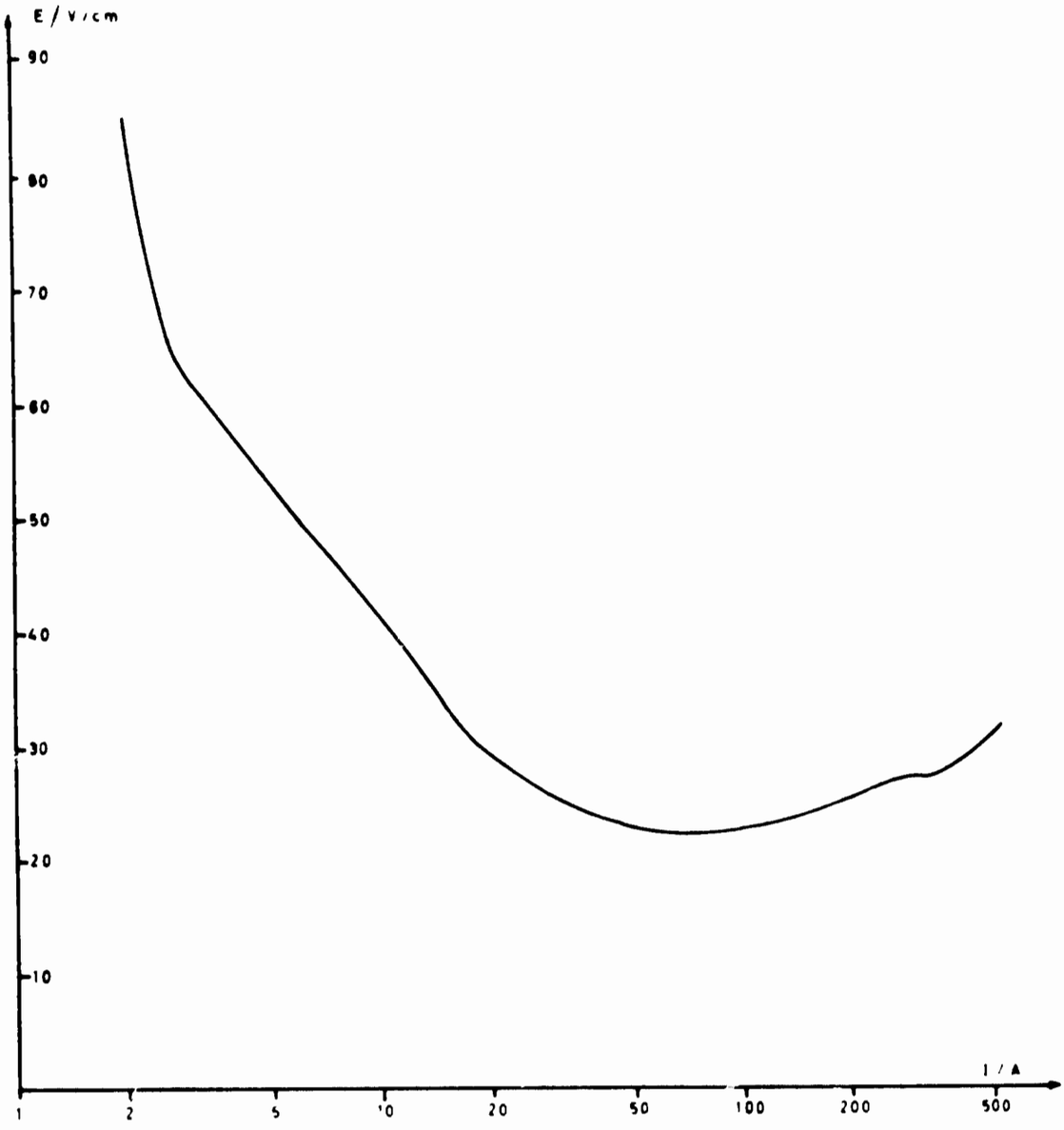

Fig. 3 : E(I) characteristic of N_2-arc measured in a tube of 5 mm diam.

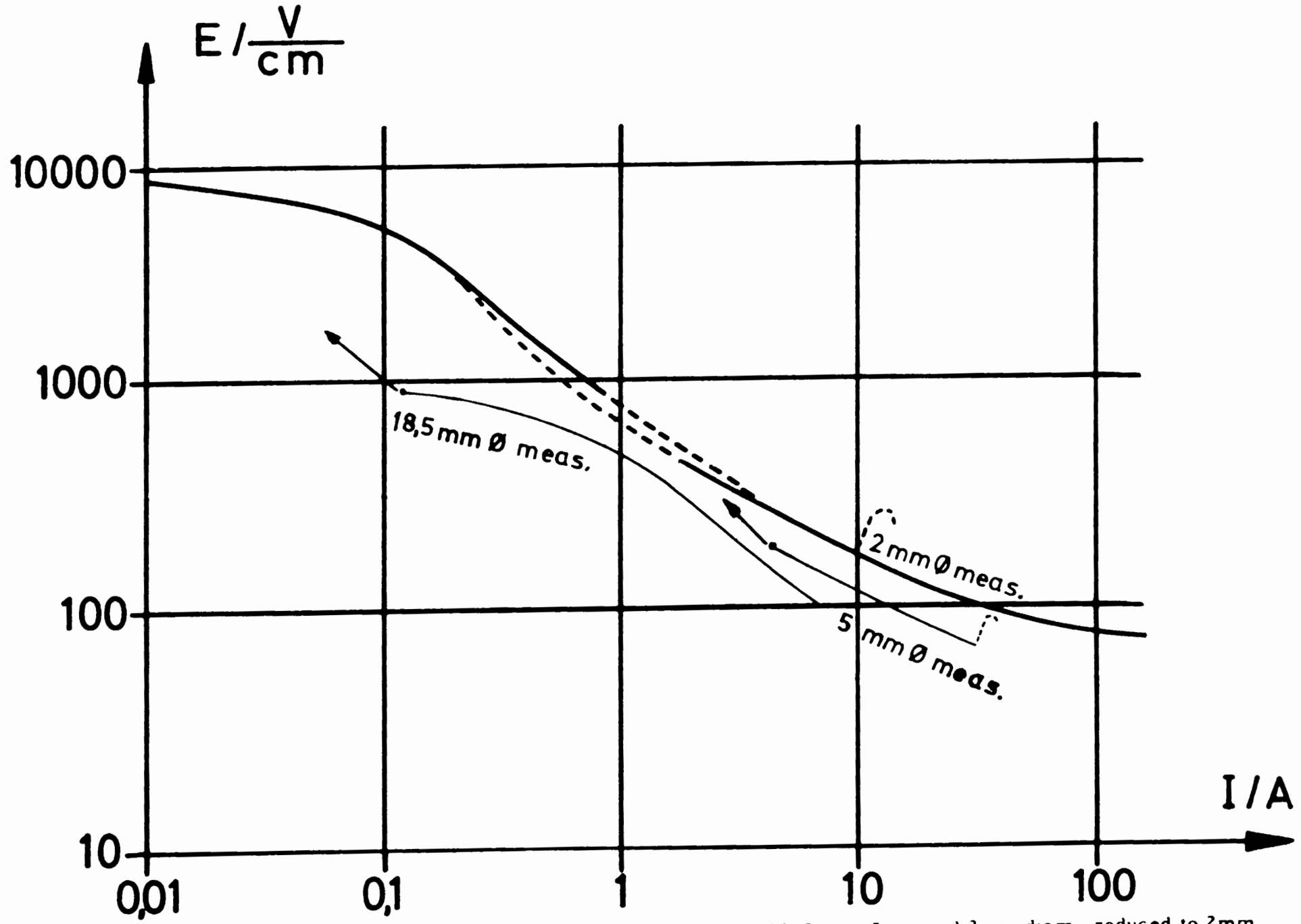

Fig. 4 : E(I) Characteristic of H_2-arc measured in tubes of 18, 5 mm, 5mm and 2mm diam. reduced to 2mm by means of scaling laws.

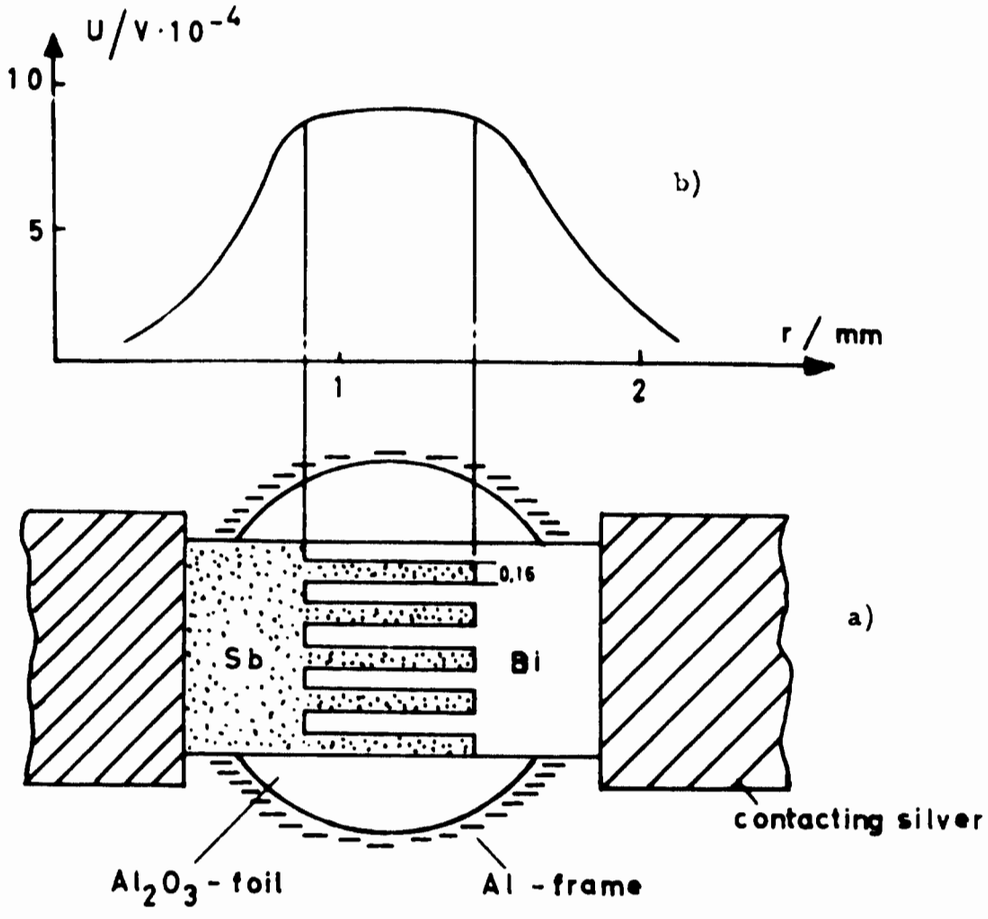

Fig. 5 : a) Scheme of the radiation thermo-couple

b) Sensitivity of the thermo-couple as a function of the locus of incident radiation

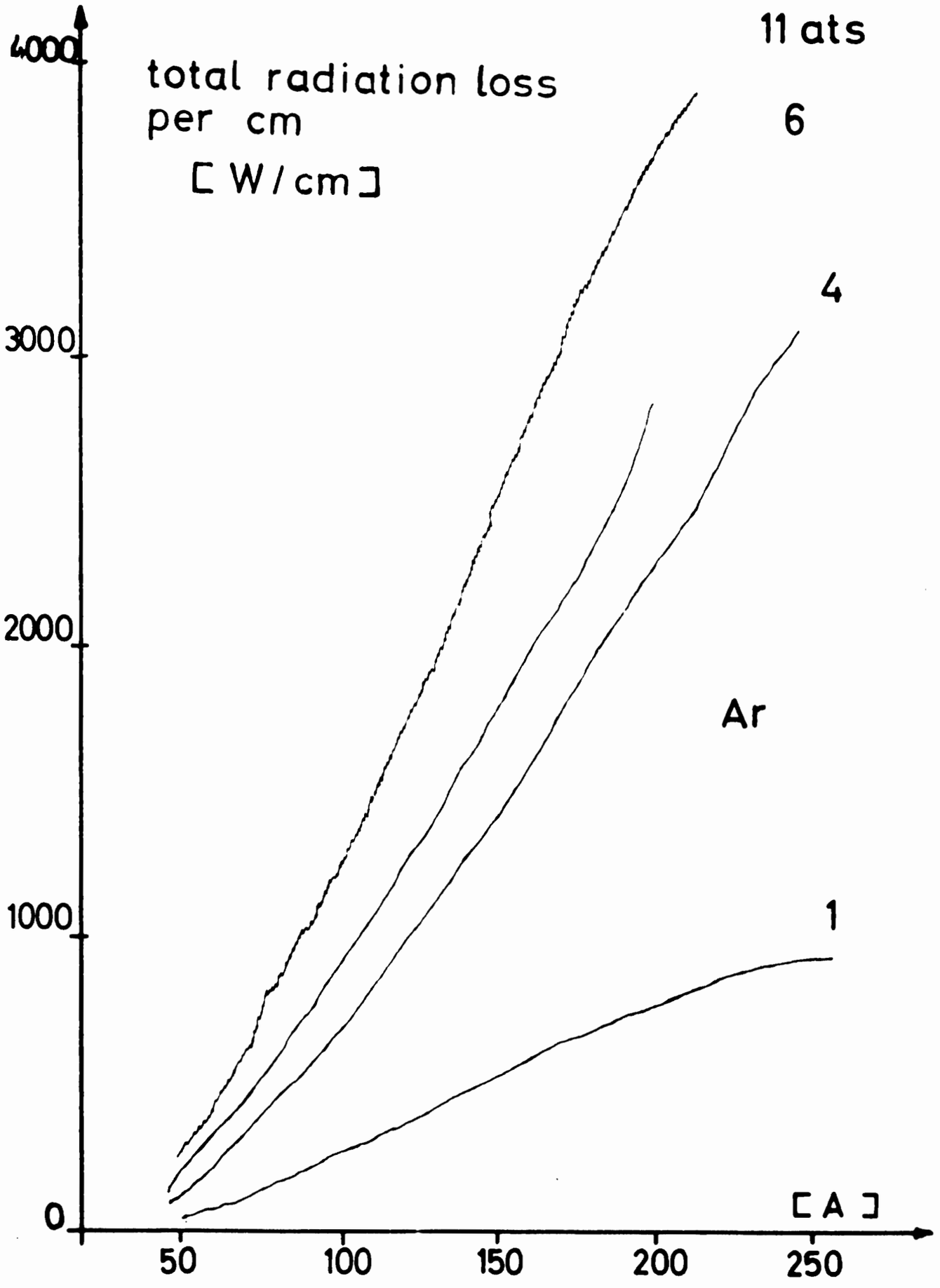

Fig. 6 : Recorder plottings of total radiation loss versus arc current.

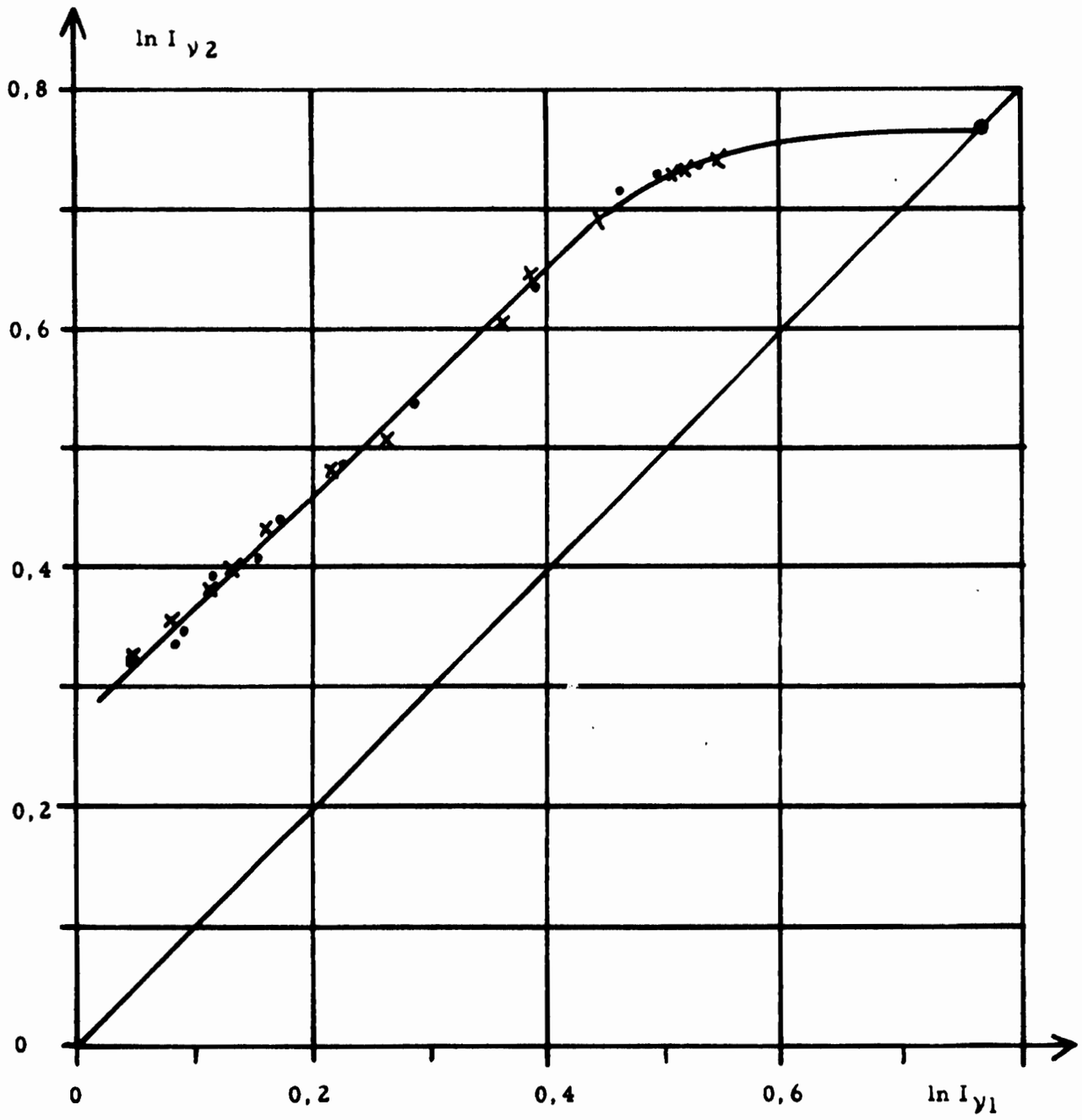

Fig. 7 $I_\nu(l_2)$ **vs.** $I_\nu(l_1)$ **within the line A II 4348 A plotted in a logarithmic system.**

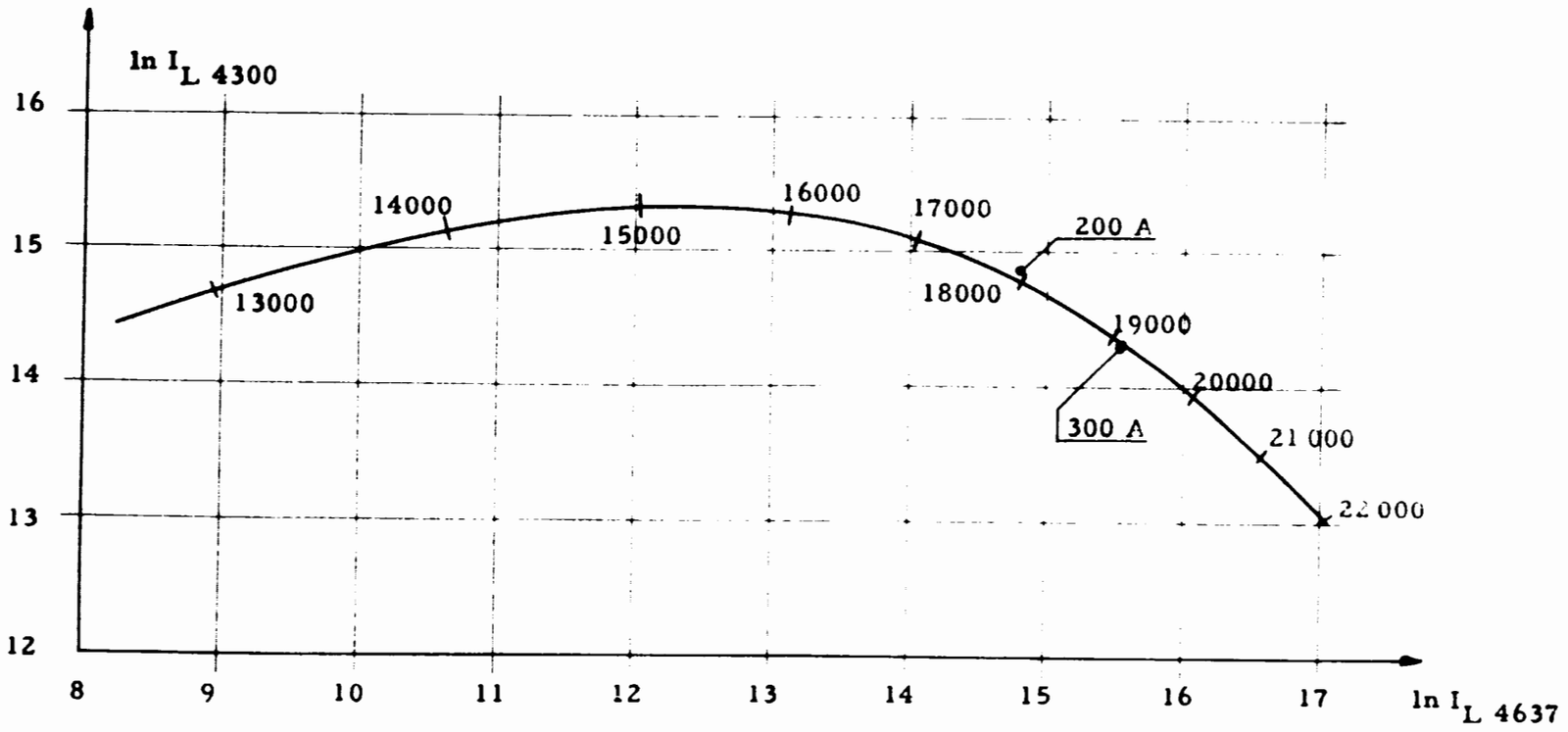

Fig. 8 ln $I_{K\ 4300}$ **vs.** ln $I_{L\ 4637}$ **with temperature as parameter**

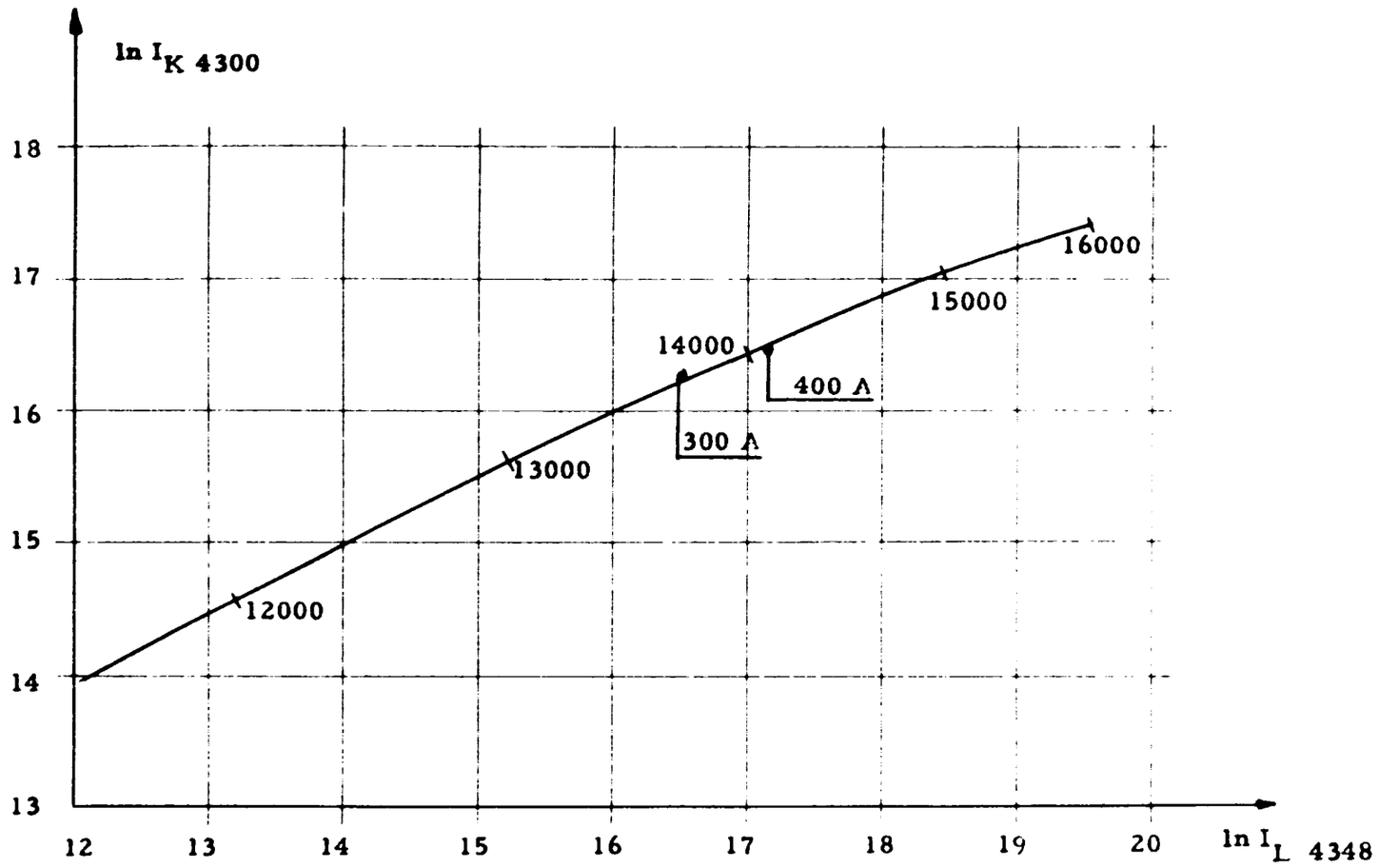

Fig. 9 ln $I_{K\,4300}$ vs. $I_{L\,4348}$ with temperature as parameter.

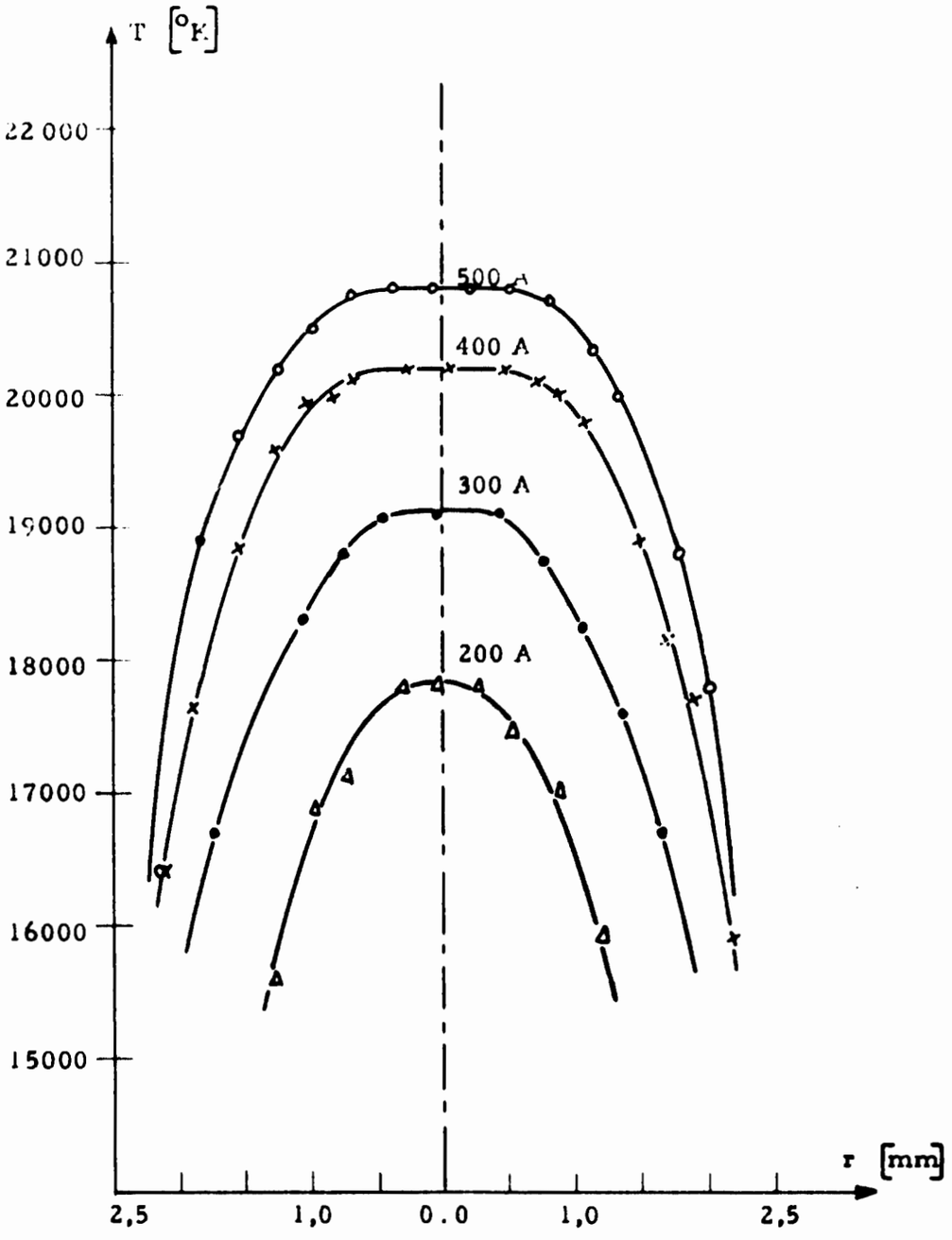

Fig. 10 Radial temperature distributions in a 5 mm diam. Ar-arc at 1 atm.

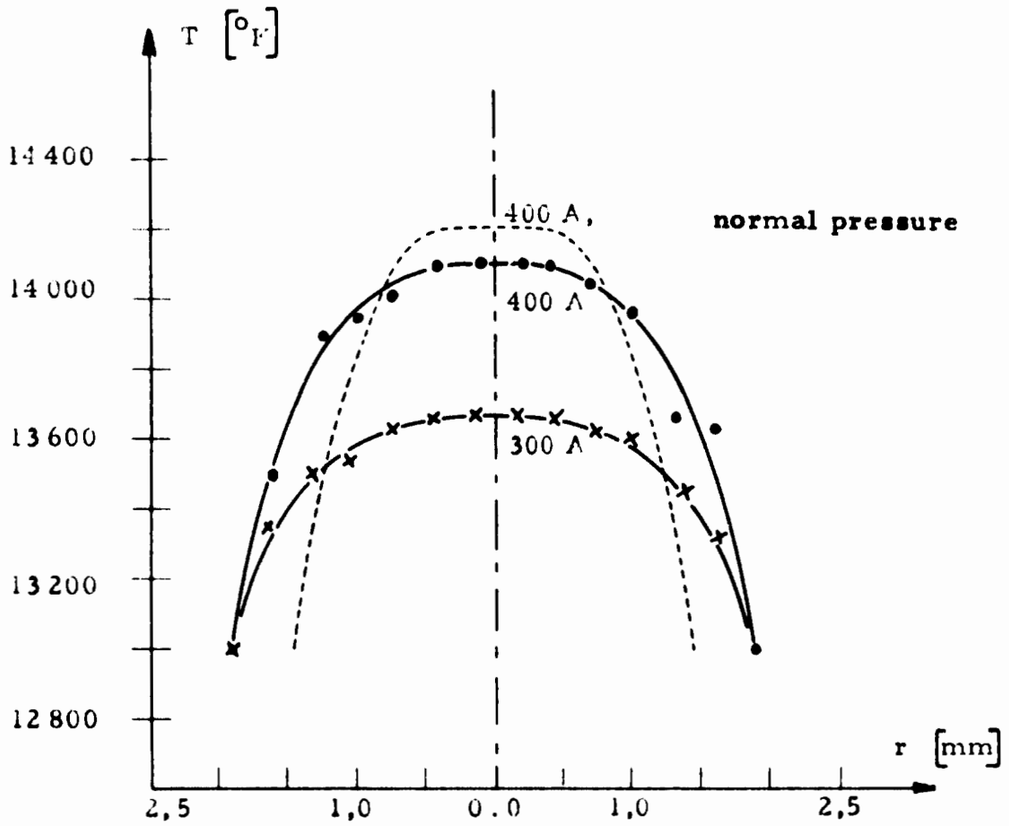

Fig. 11 **Radial temperature distributions in a 5 mm diam. Ar-arc at 5 atm.**

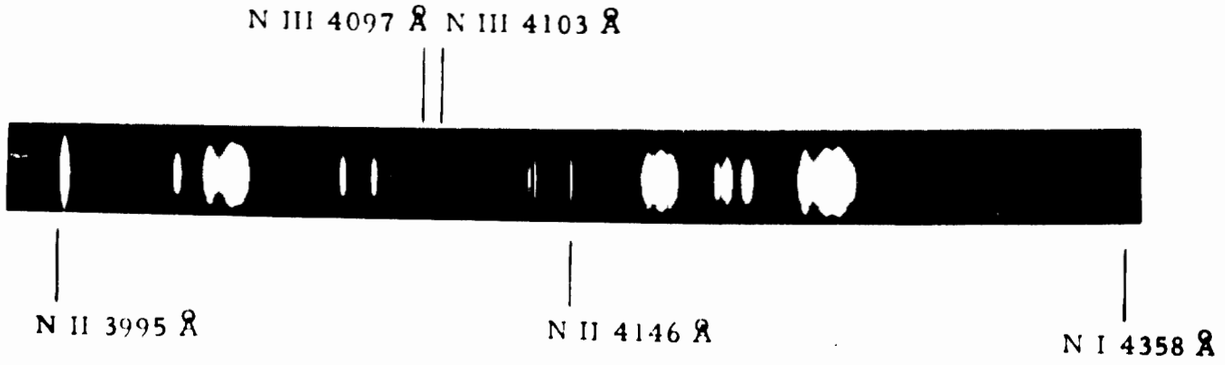

Fig. 12: Cross-spectrum of the 5 mm diam. N_2-arc at 55o A with N I, N II and N III-lines

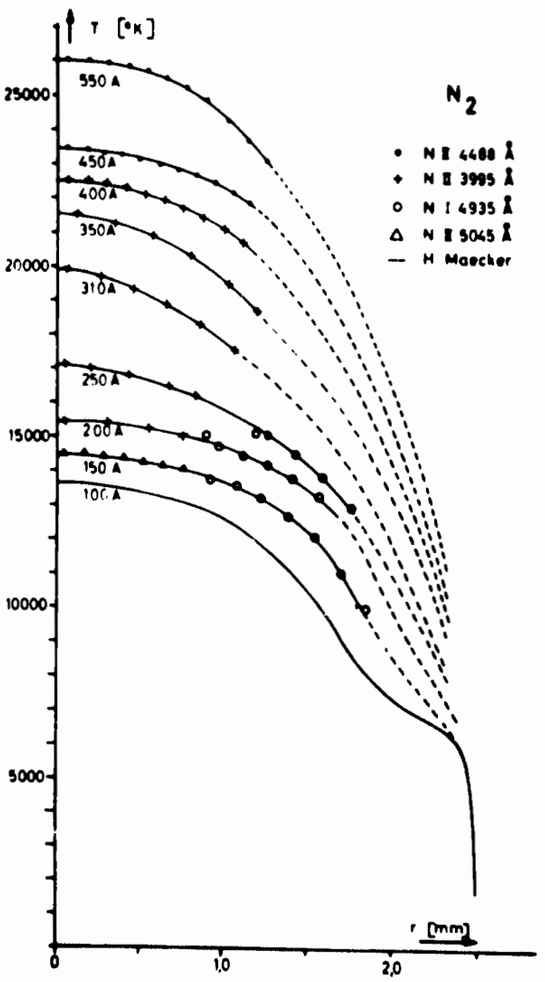

Fig. 13: Radial temperature distributions in the 5 mm diam. N_2-arc.

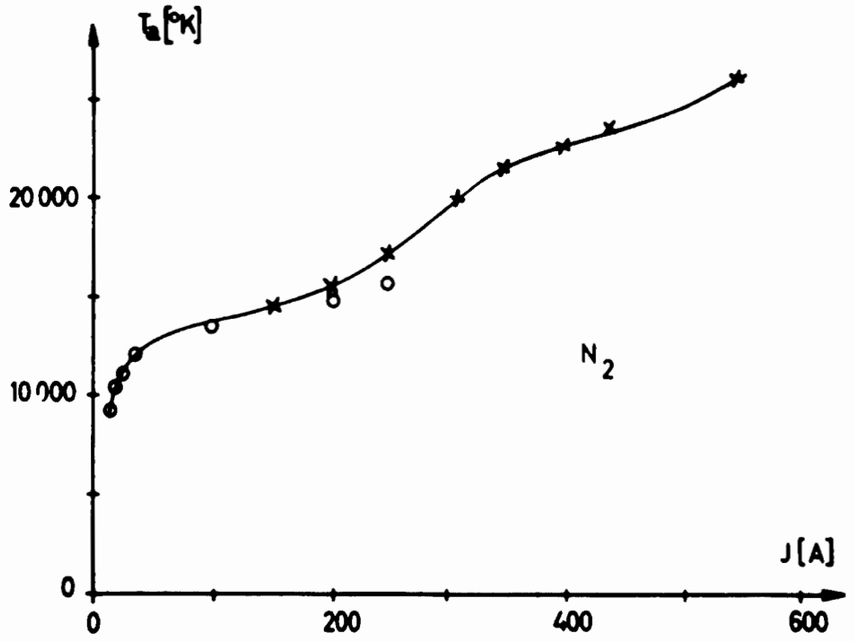

Fig. 14: Axial temperature in the N_2-arc in dependence of current

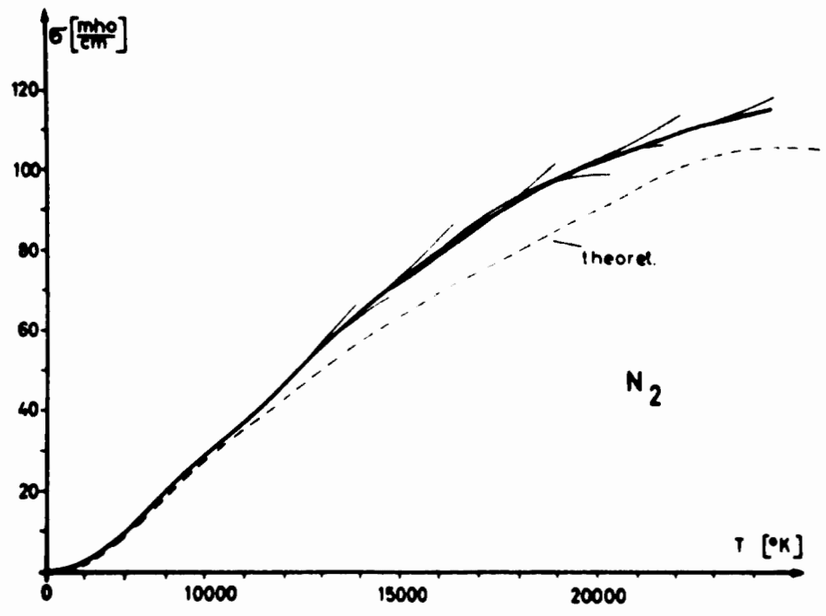

Fig. 15: Electrical conductivity in N_2 σ_{N_2} as function of temperature

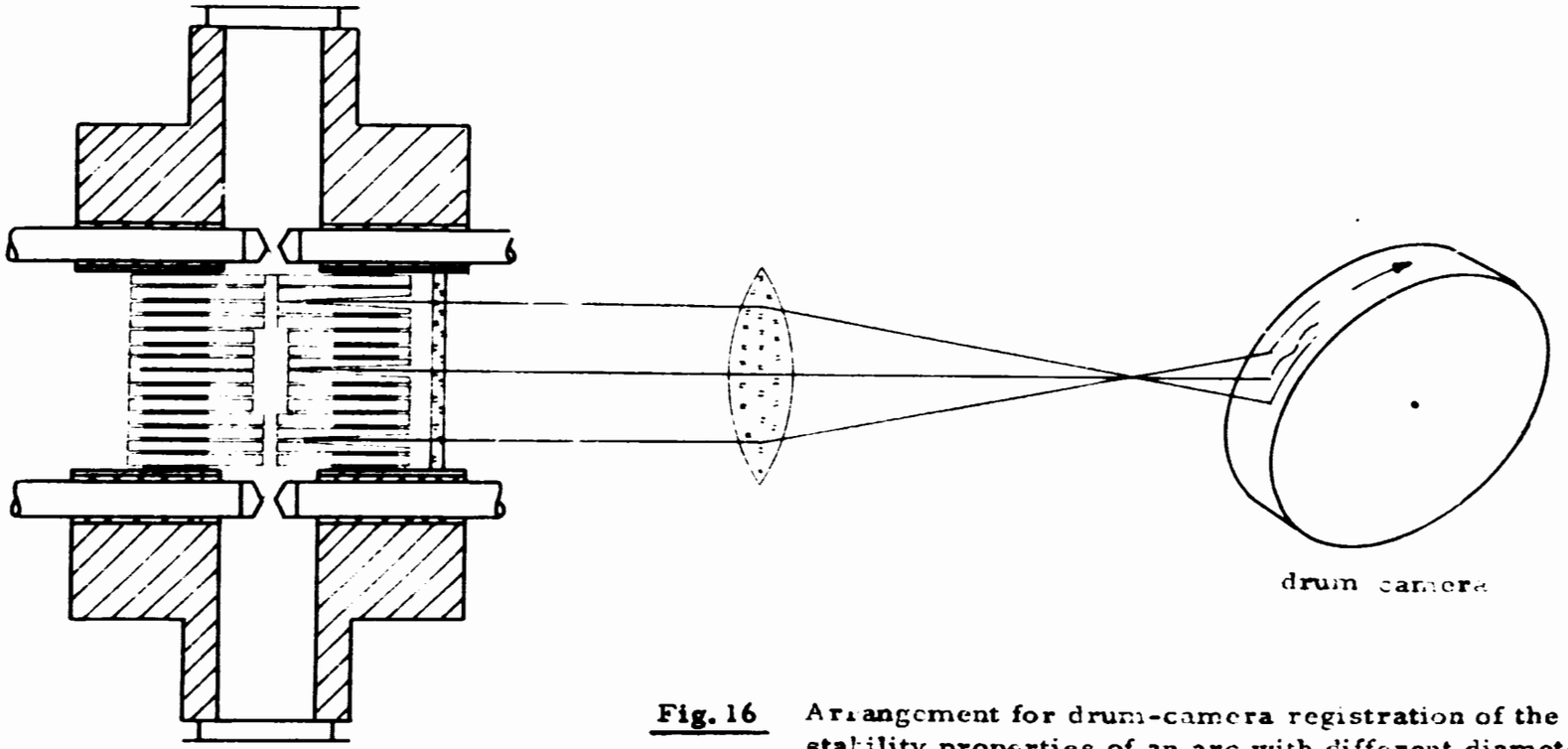

Fig. 16 Arrangement for drum-camera registration of the stability properties of an arc with different diameters.

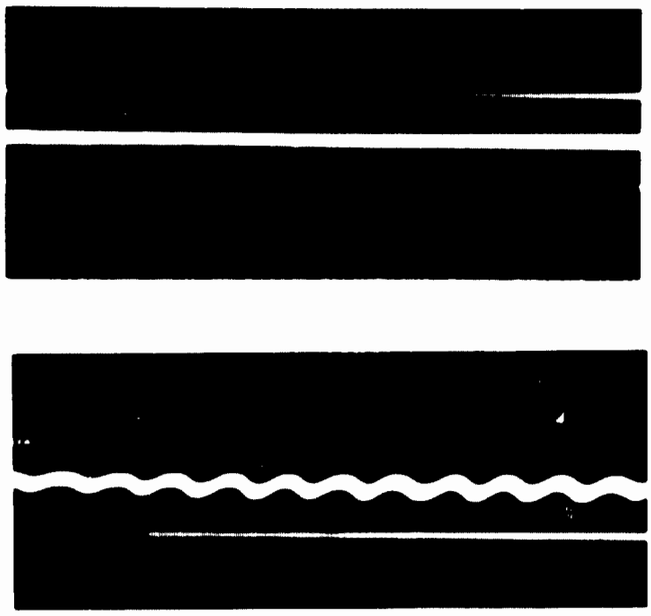

Fig. 17: Drum camera photographs of the three adjacent arc cross-sections.

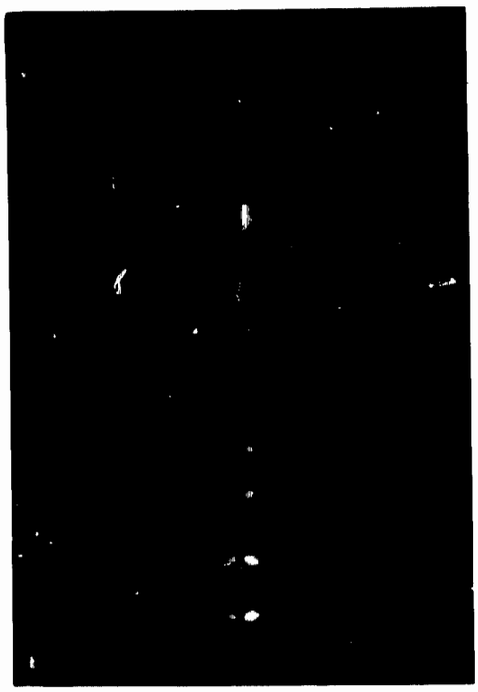

Fig. 19 H_β in end-on observation for various arc currents. Notice the depening in λ-direction connected with line broadening and the depression in r-direction due to the maximum in fig. 18

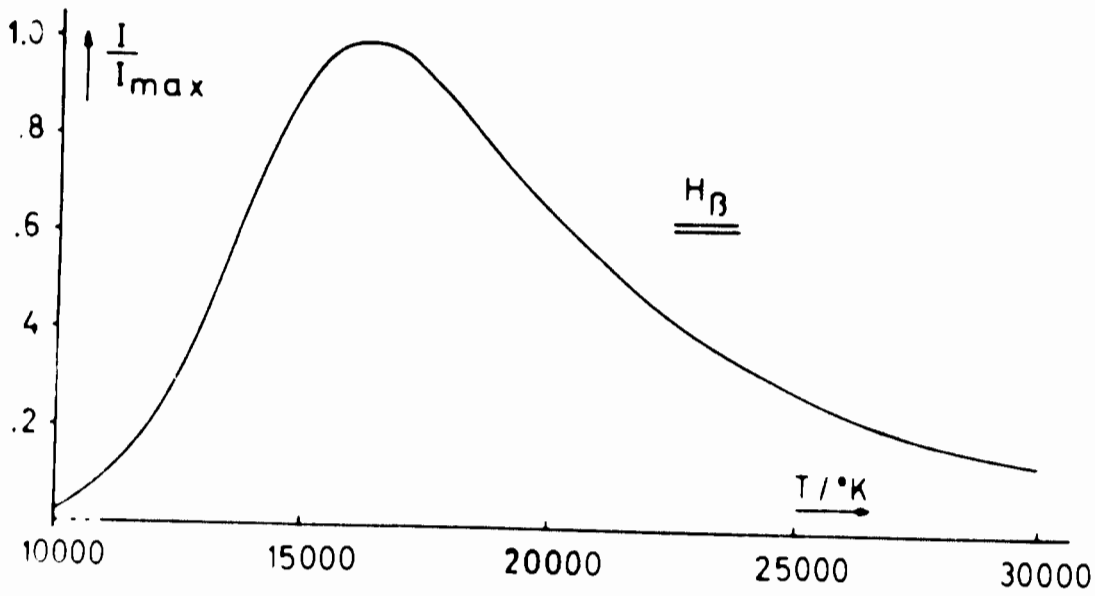

Fig. 18 Line intensity of H_β related to its maximum as function of temperature.

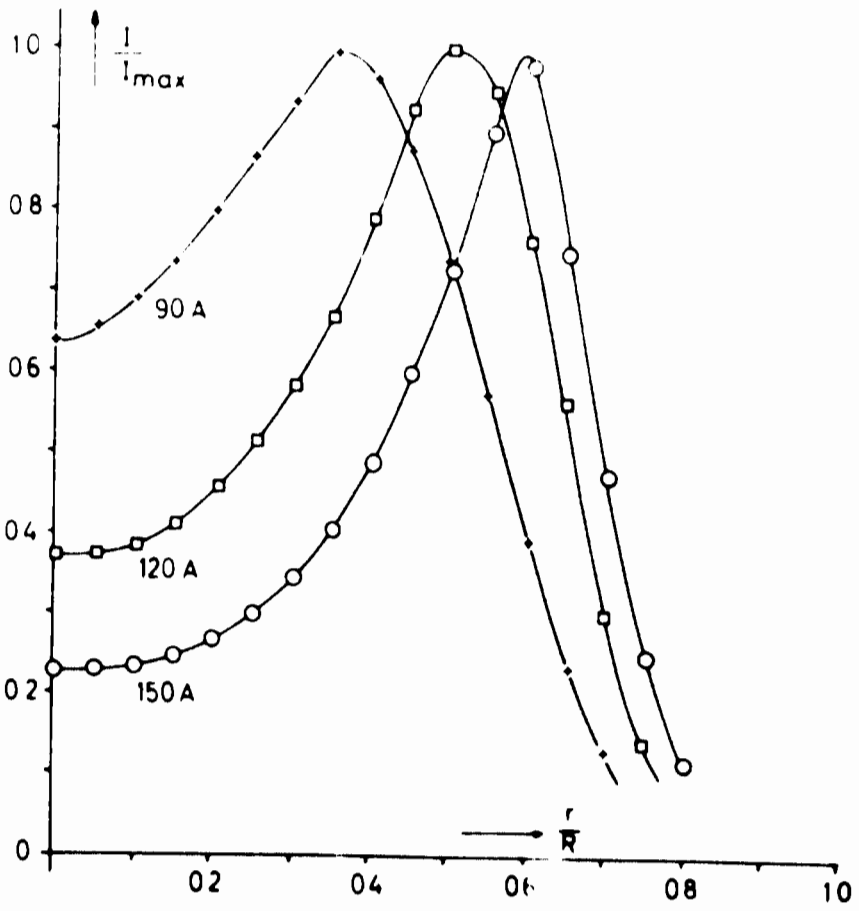

Fig. 20 Total intensity of H_β related to the maximum as function of radius for various currents.

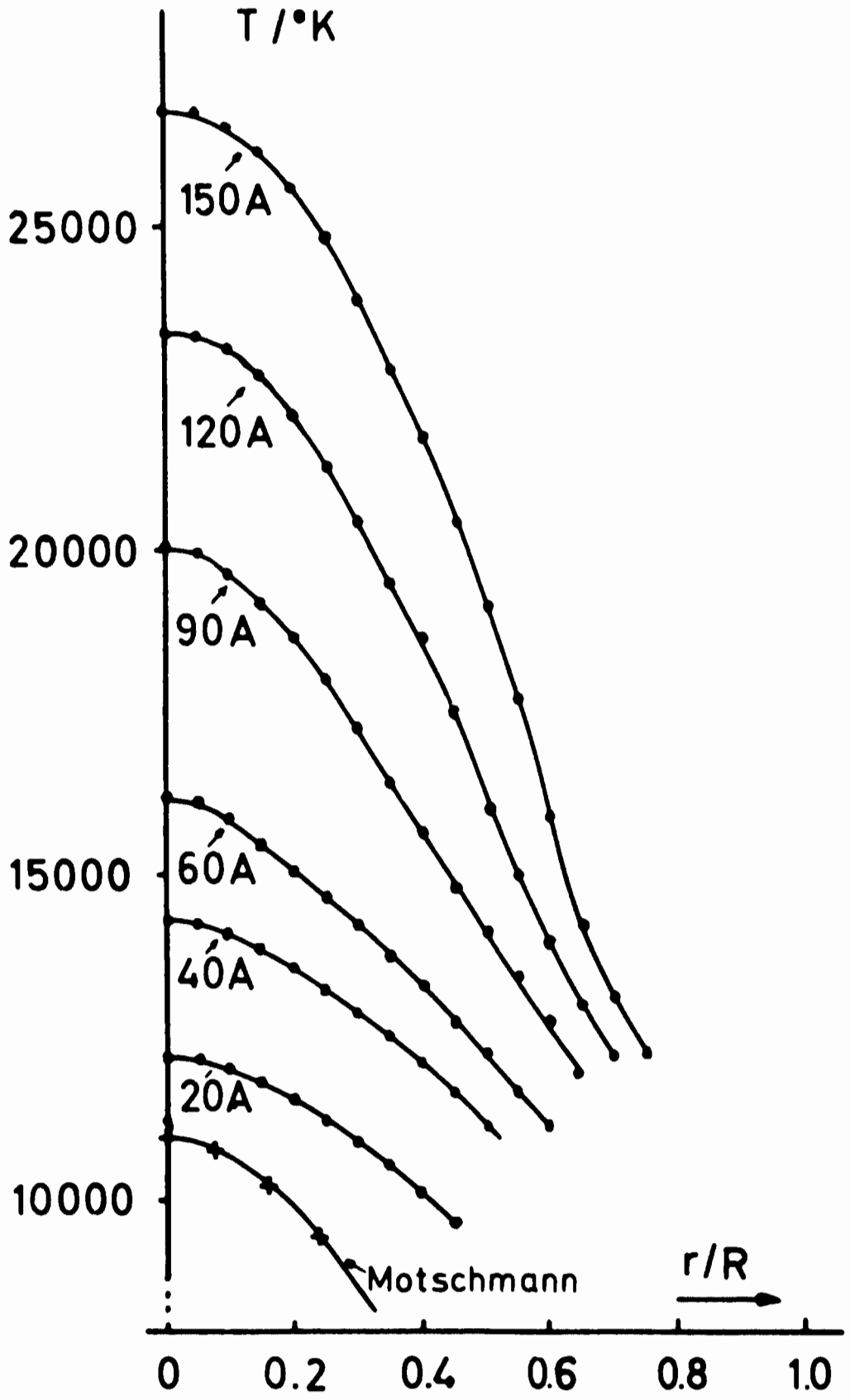

Fig. 21 Radial temperature distributions in the H_2 - arc for various currents.

Unclassified

Security Classification

DOCUMENT CONTROL DATA - R & D

(Security classification of title, body of abstract and indexing annotation must be entered when the overall report is classified)

1 ORIGINATING ACTIVITY (Corporate author)

Elektrophysikalisches Institut der Technischen Hochschule München Germany

2a. REPORT SECURITY CLASSIFICATION: Unclassified

2b. GROUP

3 REPORT TITLE

METHODS FOR DETERMINATION OF TRANSPORT COEFFICIENTS FROM HIGH POWER ARCS

4 DESCRIPTIVE NOTES (Type of report and inclusive dates)

FINAL SCIENTIFIC REPORT

5 AUTHOR(S) (First name, middle initial, last name)

Maecker, Heinz as principle investigator

6. REPORT DATE	7a. TOTAL NO OF PAGES	7b. NO OF REFS
21. October 1967	47	5

8a. CONTRACT OR GRANT NO	9a. ORIGINATOR'S REPORT NUMBER(S)
AF 61(052)-649	
b PROJECT NO.	
c.	9b. OTHER REPORT NO(S) (Any other numbers that may be assigned this report)
d	

10 DISTRIBUTION STATEMENT

11 SUPPLEMENTARY NOTES	12 SPONSORING MILITARY ACTIVITY
	Aerospace Research Laboratories

13 ABSTRACT

An improved cylindrical cascade arc chamber is described in which any gas can be heated up to full ionization and more. A distant pair of cascade discs may be used for measuring the voltage drop between them yielding the characteristic E(I). For the determination of the radiation loss a new fast recording thermo-couple has been developed. Methods for measuring the radial temperature distribution arc discussed and applied to several gases. In the argon arc absolute line intensities were determined spectroscopically by end-on observation. In this case the influence of the inhomogeneous layers and especially at elevated pressures the selfabsorption has to be regarded. The N_2-arc is observed side-on because of which ABEL's inversion has to be employed. For the H_2-arc a tube diameter of 2mm was used to overcome the arc instabilities. The measurements of temperatures in this arc were carried out by means of the relative intensity method by LARENZ with a new procedure for the determination of the total line int-ensity. Temperatures up to 26 000 °K and degrees of ionisation of more than 100 % meaning partially double ionisation have been achieved in these arcs.

The reduction of the measured results is performed by means of a step-procedure yielding a series of transport functions, namely electrical conductivity $\sigma(T)$, heat flux potential $S(T)$, thermal conductivity $\lambda(T)$ and radiative emissivity $u(T)$ without absorption, all as functions of temperature. At higher levels of current and temperature radiation absorption within the arc has to be taken into account which is discussed in detail. From the transport coefficients the involved cross-sections can be derived using the relevant transport equation of the kinetic gas theory which are given in a form appropriate for these purposes. Thereby both experimental and theoretical procedures are available to determine transport coefficients of high temperature plasmas.

DD FORM 1 NOV 68 1473

Unclassified

Security Classification

14 KEY WORDS	LINK A		LINK B		LINK C	
	ROLE	WT	ROLE	WT	ROLE	WT
Plasma						
Arc						
Cascade Arc Chamber						
Temperature Measure ment						
Electrical Conductivity						
Thermal Conductivity						
Radiative Diffusion						
Transport Coefficients						
Cross-Sections						